COPPER KING PROPERTY
INDUCED POLARIZATION SURVEY
GIS DATABASE

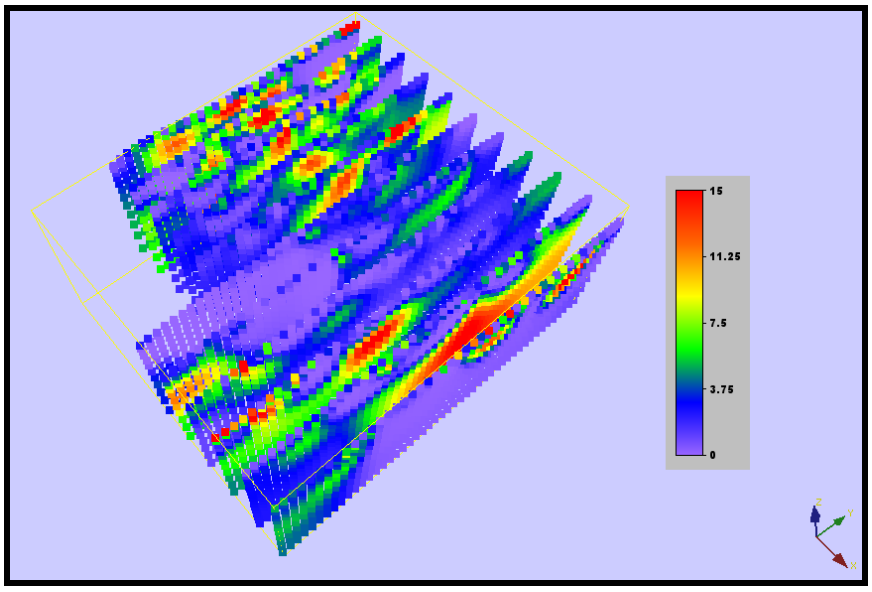

Inverted Chargeability Stacked Sections Looking Northwest

James L. Wright M.Sc.
November 5, 2017

TABLE OF CONTENTS

INTRODUCTION

From Oct. 13 to 30, 2017 an induced polarization (IP) survey was completed over the Copper King property controlled by U. S. Gold Corporation. Objective was to delineate sulfide concentrations via the chargeability and lithologies via the resistivity. Copper mineralization, revealed by historic mining in the area, indicates IP would be the appropriate technique for detection of similar material. Structural and lithologic information, generated mostly by the resistivity parameter, is combined with data from a previous magnetic survey (Wright 2017) to yield a refined analysis of the property.

Survey procedures are reviewed first followed by a description of data processing and an interpretation, and finally conclusions / recommendations. Results of the survey are presented in both map form and MAPINFO / ARCGIS GIS files. The GIS files are contained on a DVD located in a folder at the rear of the report. Also contained on the DVD are regional data files, digital files for the survey, as well as a copy of the report. In fact, a complete GIS database is located on the DVD. A README file clearly defines the various folders and files. Map products are also provided as digital SRF plot files as listed in the Table of Contents.

Figure 1 shows the property's location relative to Laramie and Cheyenne, Wyoming.

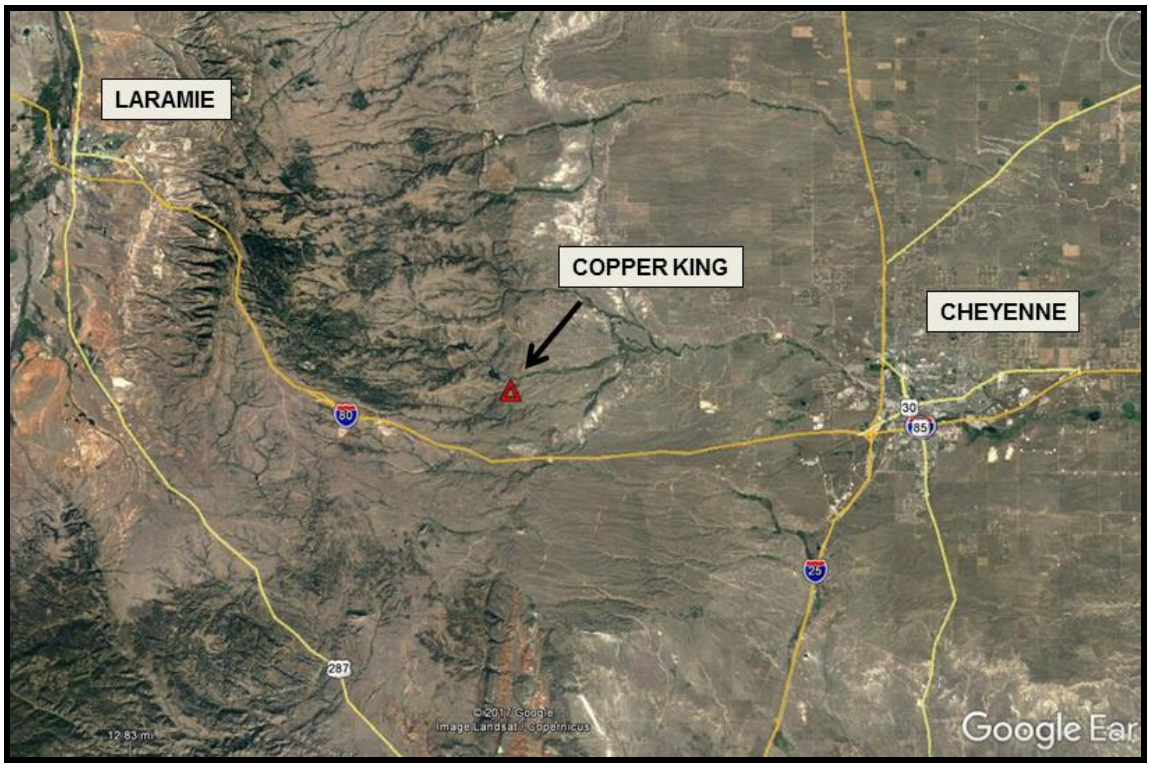

FIGURE 1: Copper King Property Location

SURVEY PROCEDURE

Figure 2 shows the IP lines over topography. Line numbering is based upon the **NAD 27 / UTM 13N** easting, the coordinate system used for all work on the property.

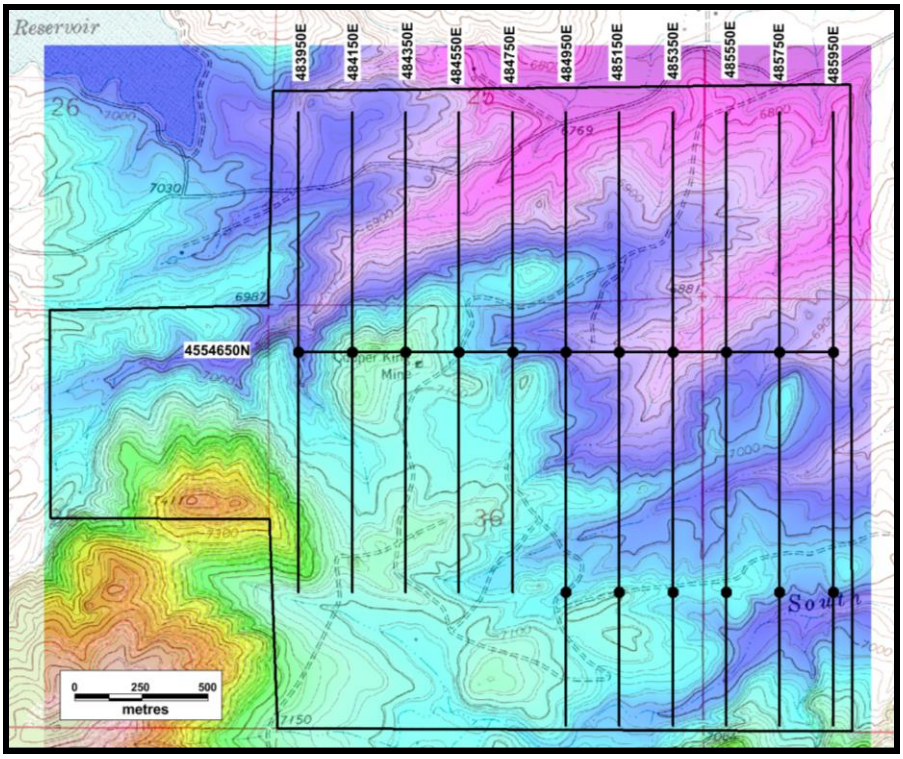

FIGURE 2: IP Lines, Property Boundary over Topography

Zonge Geosciences, Inc. based in Reno, Nevada acquired the eleven lines if IP data using a dipole-dipole electrode array with a 100m dipole length. Measurements were made for n-spacing of 1 through 11, using standard 9-electrode spreads on all lines. Data were acquired in the time-domain mode with a fundamental frequency of .125 Hz. Marco Zamudio, Geophysical Crew Chief for Zonge International conducted survey operations under Zonge job number 17053.

Stations were located using a Garmin hand-held GPS, model GPSMAP 64CSx. The GPS data were differentially corrected in real-time using WAAS corrections. Accuracy of the GPSMAP 60CSx typically ranges from 2-5 meters. Line control in the field utilized UTM 13N / NAD27 coordinate system. Topography data were extracted from 10 meter digital elevation model (DEM) files.

Instrumentation consisted of a Zonge model GDP-3224 multiple purpose receiver. The electric-field signal was measured at the receiver site using non-polarizing ceramic porous-pot electrodes connected to the receiver with insulated 14-gauge wire. The signal source for the IP measurements was a Zonge GGT-10 transmitter, serial number 558A.

The GGT-10 is a constant-current 10 KVA transmitter. Power for the transmitter was provided by a Zonge ZMG-9, 9 KVA motor-generator with an external voltage regulator. A replacement Zonge ZMG-30DL motor-generator was mobilized to the project and arrived on October 16th. The Zonge ZMG-30DL motor-generator is 30 KVA generator which is equipped with a built-in voltage regulator. The transmitter was controlled by an XMT-G GPS transmitter controller, serial number 9EB5. Transmitter-receiver synchronization was maintained via GPS signal. Instrument specifications are included with the digital data release. Measurements in the field demonstrated good repeatability and IP error values are less than one msec. Additional survey logistical details are available in Appendix A.

DATA PROCESSING

Numerical data for the IP survey included apparent resistivities in ohm-meters (ohm-m) and chargeabilities as Newmont standard values in milliseconds (msec). These data were provided in two text files (.avg and .stn) for each of the eleven lines. The AVG files contained the averaged and edited data, and the STN file contains the station survey locations in UTM 13N / NAD 27 coordinates. Data quality for the entire survey is good and required minimal data editing.

The dipole-dipole data received complete 2D inversions for both the chargeabilities and resistivities. The processing flow commenced with verifying conversion of the data to the proper format for input to the Zonge TS2DIP 4.20g smooth model Res / IP inversion program followed by inversion. Appendix B contains inversion / model summaries for each line. The top image shows the inverted model, below are the observed and calculated data base upon the model. The data are arranged by line in the IP folder on the accompanying DVD.

The IP inversion model for a given line extends laterally from the outer electrode / pot locations to a depth of approximately two dipole lengths determined by the 1% sensitivity limit (see Appendix B). Within the model are discretization blocks ranging from half dipole width near surface to approximately 50 m height at depth.

Prior to processing, the resistivity data were converted to logarithms base ten. The gridded resistivity and chargeability inverted data were colored and contoured with intervals of 0.1 and 1 respectively. Color bars for the resistivity and chargeability follow. This color palette and contour intervals apply to all products, both map and GIS.

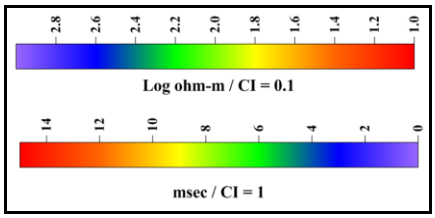

MAPINFO and ARCGIS files for the inverted sections with contours embedded were generated by rotating sections to the east about the line trace into plan view and are

located on the DVD. Appendix C contains numerous example of the rotated section format. Map slices for the 0 – 50 m, 50 – 100 m, 50 – 150 m and 100 – 200 m **depth** intervals were developed for both the chargeability and resistivity using the same coloration and contour intervals as the sections. It is important to note these are depths below surface intervals and not fixed elevations. Plots files at 1:5000 scale for both the slices and sections are located on the DVD. Examples of the SRF plot files for the sections and depth slices follow.

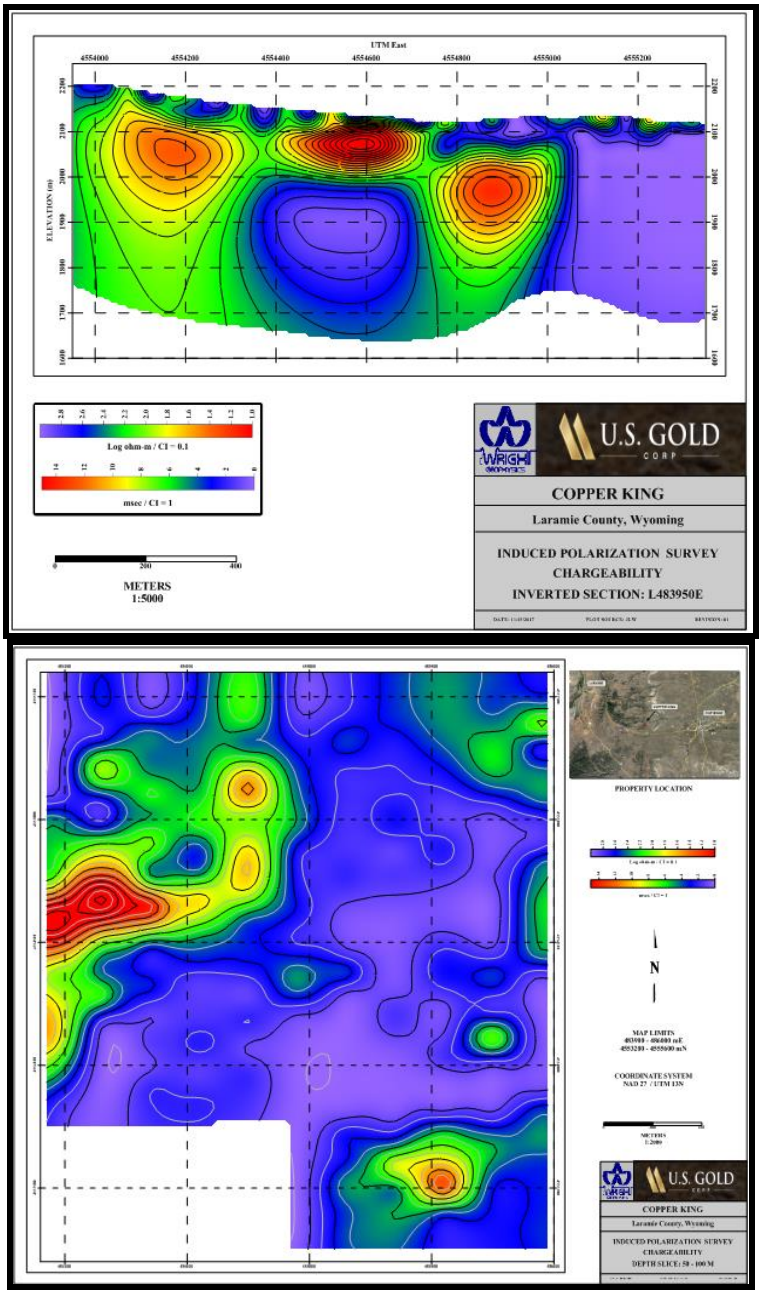

FIGURE 3: Example Section and Depth Slice Plots

All the section inversions were combined and imported into the VOXLER three dimensional visualization software. Figure 4 presents an example from the program.

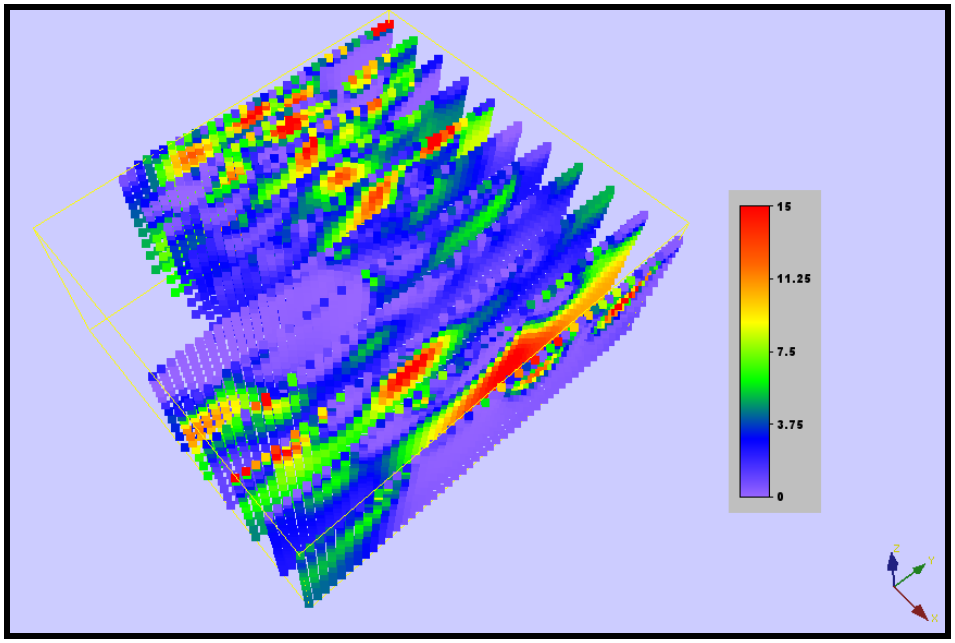

FIGURE 4: Inverted Chargeability Stacked Sections Looking Northwest

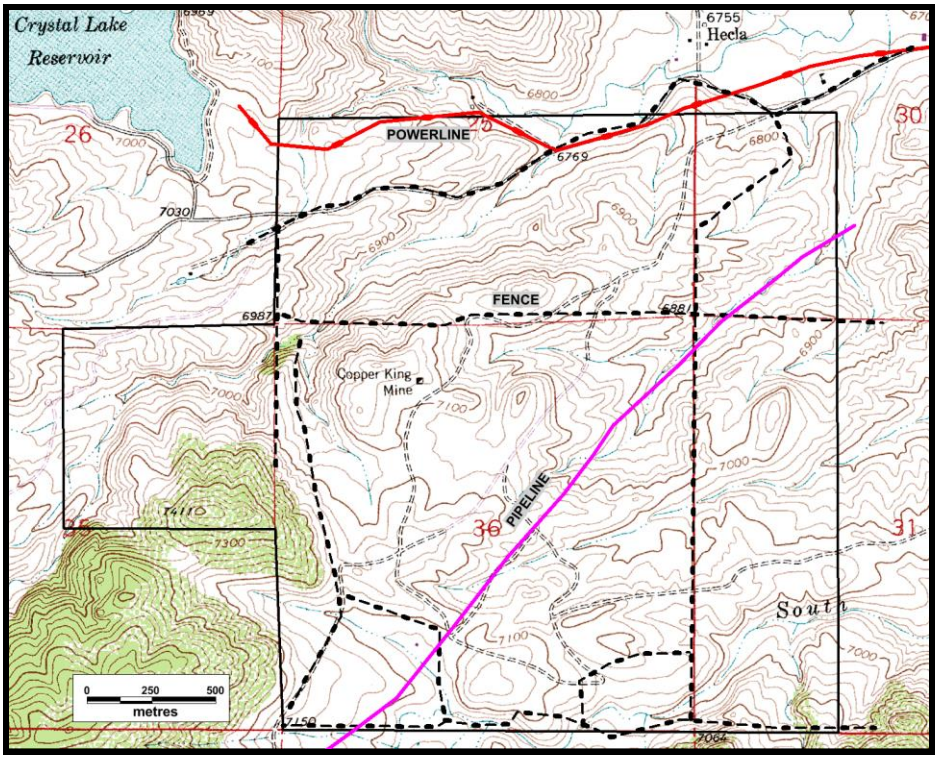

FIGURE 5: Cultural Features over Topography

A number of cultural features were encountered in and around the survey area. These include fences, a power line and pipe line. Figure 5 shows the various features over topography. Fortunately, none of these impacted the survey in any significant way.

INTERPRETATION

In June 2017 a ground magnetic survey was completed over the property as historic data indicated a strong correlation of mineralization with a magnetic anomaly. In fact, geologic observations confirmed the correlation of gold mineralization with magnetite. The magnetic survey is reviewed by Wright (2017) where the gold / magnetic correlation is confirmed and quantified. Historic geologic reports also note induced polarization chargeability responses correlate with the known mineralization. Appendix C presents both the resistivity and chargeability sections over the residual, reduce to pole (RTP) magnetics for all eleven lines. Figure 6 shows an example of the sections in Appendix C.

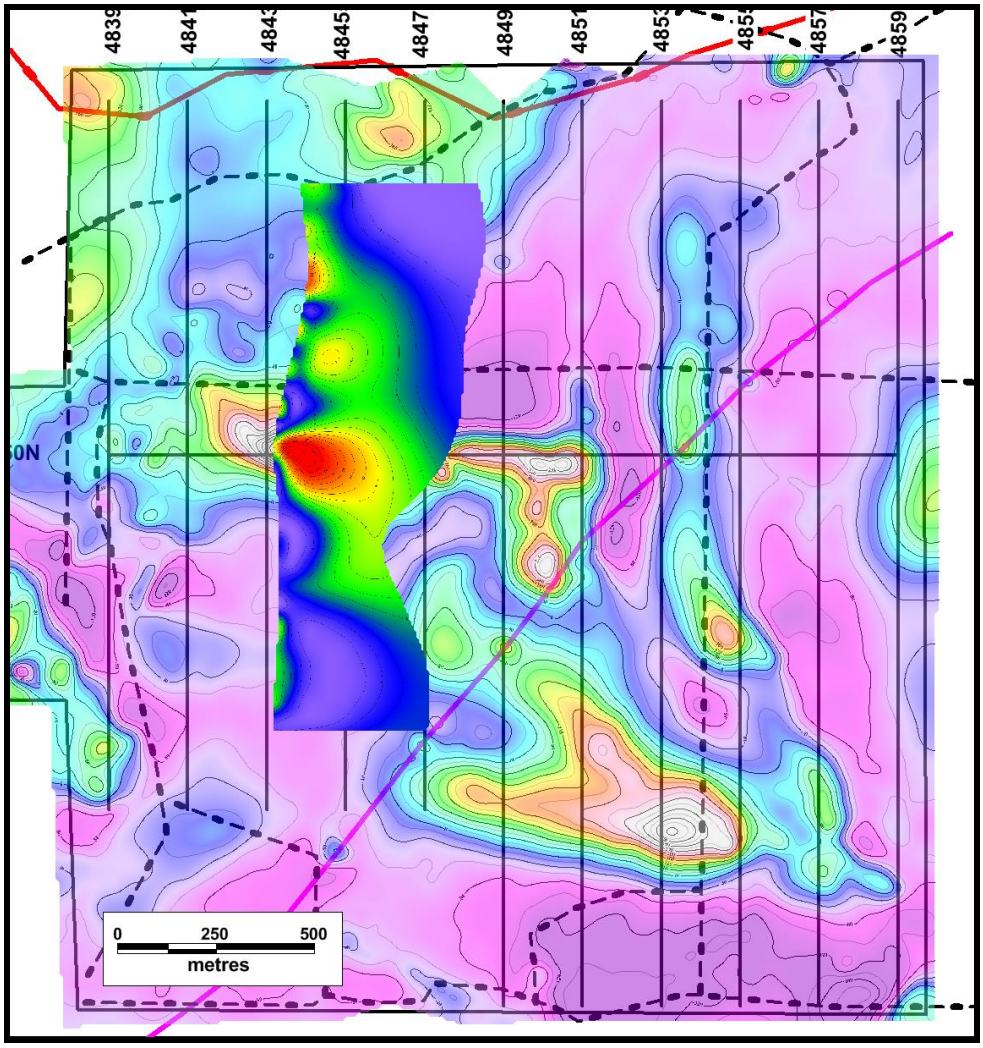

FIGURE 6: Line 484350E Chargeability Section over RTP Residual Magnetics

As Figure 6 confirms, a moderate strength chargeability anomaly correlates directly with the known mineralization and prominent magnetic anomaly. Each of the lines is discussed briefly in the following.

L483950E: The resistivity section is dominated by high values approaching 1000 ohm-m across the southern three quarters of the section. Lower values cover the extreme north portion of the section being bounded on the south side by a possible high angle structure. Three moderate strength chargeabilities areas occur along the section within a very low background. None appear to be related to cultural features such as the fences. The center anomaly is the extreme western extension of the prominent anomaly associated with the known mineralization. In addition, the anomaly is associated with moderate strength magnetic responses.

L484150E: High resistivity values correlate with elevated magnetics east of the main ore zone. These are an eastern extension of the high values noted on L483950E, which suggests a form of alteration. Low resistivity values dominate to the south and north of this zone. Exactly coincident with the resistivity / magnetic high is a tabular, moderate strength chargeability anomaly. Thickness of cover is minimal with the source likely outcropping. A smaller, near surface anomaly is noted on the north edge of the coverage. A third deep anomaly occurs south of the main zone response; however, this anomaly has no magnetic correlation and is suspect due to the unusual shape of the response. In addition, close examination of the inversion results (see Appendix B) does not reveal a source for the anomaly in the observed data.

L484350E: This section traverses the center of known mineralization. As with the previous sections, a prominent high resistivity zone correlates with elevated magnetics and is flanked to the north and south by low resistivity material. A low resistivity layer starts immediately south of the mineralized zone and is interpreted to be produced by overburden. A prominent chargeability anomaly correlates directly with the known mineralized zone and associated strong magnetic high. The chargeability anomaly plunges at high angle to the south. Two smaller scale anomalies are located to the north in the broad zone of elevated resistivity.

L484550E: The aforementioned band of high resistivity persists to the north of the main mineralized zone and appears to plunge to the south. Correlation with elevated magnetic values is still evident for most of the zone's width. To the south, a low resistivity overburden layer is evident as with the previous line. A prominent chargeability anomaly is evident plunging to the north with a width of approximately 250 m. Depth to top of the anomaly is on the order of 40. This is clearly the eastern extension of the main mineralized zone, perhaps beneath cover. Scattered, shallow, smaller chargeability anomalies are located north of the main response within the high resistivity band.

L484750E: The high resistivity band continues on this section; however, the correlation with elevated magnetic values is not as evident as with the lines to the west. Low resistivity values encroach over the band on the south edge and are interpreted as overburden. A prominent chargeability anomaly is noted in the center of the section

dipping steeply to the south. Width is substantial on the order of 250 m with a depth to top of approximately 40 m. A shallow moderate strength anomaly is noted north of the main response. Correlation of these two anomalies with the high resistivity band is good. Importantly, the strong chargeability response does not correlate with a magnetic anomaly.

L484950E: The prominent high resistivity band over the north half of the section is beginning to be interrupted by smaller scale low resistivity features. To the south, a prominent low resistivity surface layer has developed with suggestions of a high angle, underlying low resistivity features. Two of these high angle features bound either side of the west end of the Fish magnetic anomaly. The chargeability section is quite different from those to the west. A weak anomaly is noted on the north end of the section, which could be the end of the main zone anomaly bending to the north. The Fish magnetic anomaly and a prominent magnetic high along strike with the main zone magnetic anomaly show no chargeability correlation.

L485150E: A variable thickness, low resistivity layer extends across the entire section with the thickest portion along the southern half. An underlying, high angle, low resistivity feature is located immediately south of the Fish magnetic anomaly. High resistivities underlie the surface layer. The chargeability section is subdued with a deep poorly defined response to the north and a stronger anomaly along the south edge of the section. A small near surface response mid-section could be cultural in origin. However, the anomaly on the south end of the section is proximal to the south edge of the Fish magnetic anomaly. No chargeability responses correlate directly with any of the magnetic anomalies along the section.

L485350E: The previous line's low resistivity layer extends along the central portion of the section. Thickness varies from 20 to 50 m. Again, a high angle, low resistivity feature is noted on the southern end of the layer. On this line, the feature correlates directly with the strongest part of the Fish magnetic anomaly. The chargeability section is flat except for one response centered south of the Fish anomaly. The shallow part of this anomaly appears to be cultural, being produced by a fence. However, the deeper portion centers beneath the Fish anomaly in direct correlation with the high angle low resistivity zone.

L485550E: As with several of the previous sections, the resistivity is dominated by a low resistivity layer extending for much of the section. The layer is thin, on the order of 20 m thick. Similarly, the south end of the layer is bounded by a high angle, low resistivity feature which correlate with the eastern tip of the Fish magnetic anomaly. The chargeability section reveals two response of note. A deep anomaly is located near the middle of the section, which correlates with a shallow magnetic high. Depth to top is on the order of 150 m. However, this anomaly is not well defined by the IP coverage and will require further verification. A complex chargeability response is located on the south end of section near the east tip of the Fish anomaly. Correlation with the high angle, low resistivity feature is noted.

L485750E: The resistivity section continues to increase in complexity with a low resistivity surface layer encroaching from the north and an intermediate depth low resistivity layer extending across much of the section. A deep chargeability anomaly is positioned slightly north of section center and immediately west of a magnetic high on section 485950E. Depth to top is on the order of 200 m. A weaker chargeability anomaly is located along strike from the Fish anomaly with a weak magnetic correlation.

L485950E: A thin, near surface, low resistivity layer returns over the central third of the section with thick low resistivity dominating the northern third. The chargeability section reveals three anomalies. One is located on the extreme north end and another mid-section in direct correlation with a magnetic anomaly. The third is weak and poorly formed, but is on the strike extension of the Fish anomaly.

Sectional analysis is excellent for quantifying IP results, but is difficult to envision how the various features connect in plan. However, depth slices are well suited for connecting the interpretive elements in plan.

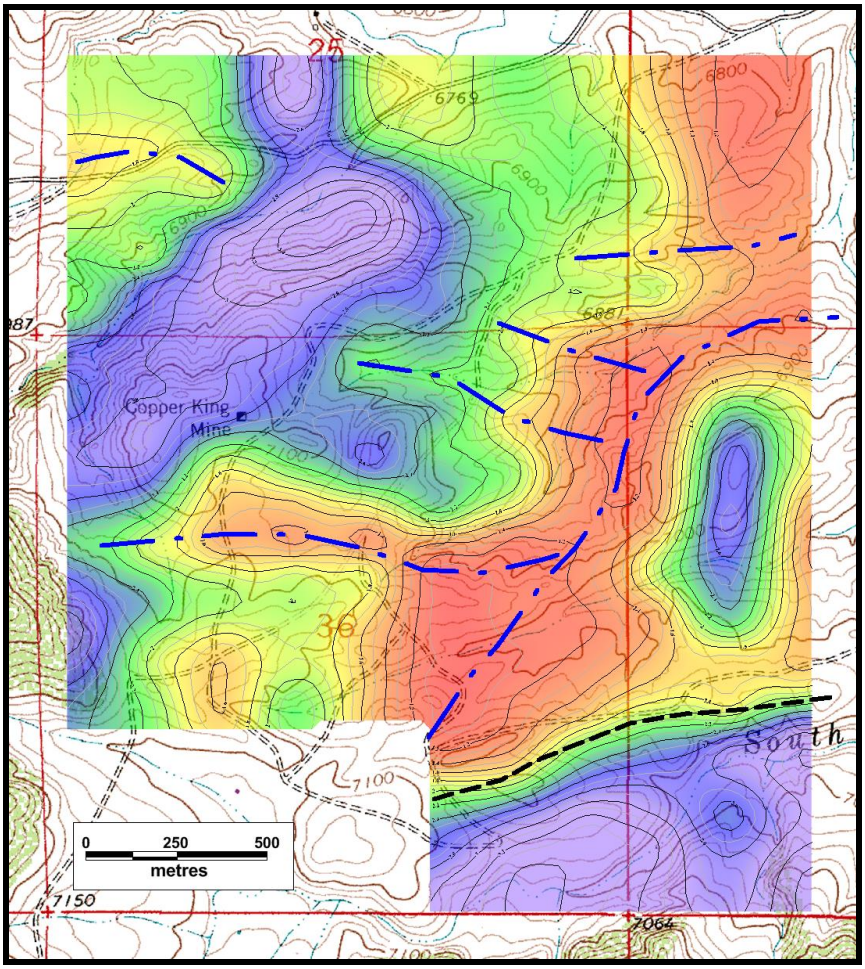

FIGURE 7: Resistivity Depth Slice 0 – 50 m over Topography

The resistivity 0 – 50 m depth slice is presented in Figure 7 over the topography. This shallow resistivity slice is dominated by overburden depth variations as noted numerous times in the section discussions. Many of the IP sections which cut the Fish magnetic anomaly indicate a low resistivity feature extending to depth off the south edge of the overburden layer. In the plan view, the southern termination of this central overburden layer is quite linear; suggesting the termination is controlled by an east-northeast oriented structure, as the dashed black line in Figure 7 indicates. This structure cuts the Fish anomaly immediately northwest of the highest magnetic response. The resistivity pattern north of this structure is typical for a network of paleo-channels in-filled with overburden. Paleo-channels are indicated with blue lines in the figure. A north-south elongated bedrock high is indicated along Line 485750E mid-section.

North and northeast of the Copper King shaft is an extensive area of high resistivity. As noted in the section reviews, this area tends to correlate with elevated magnetic and chargeability values. The elevated chargeabilities are evident in Figure 8 where the 50 – 100 m chargeability depth slice is presented over topography. Such a correlation could well be reflecting alteration extend north from the main zone at Copper King.

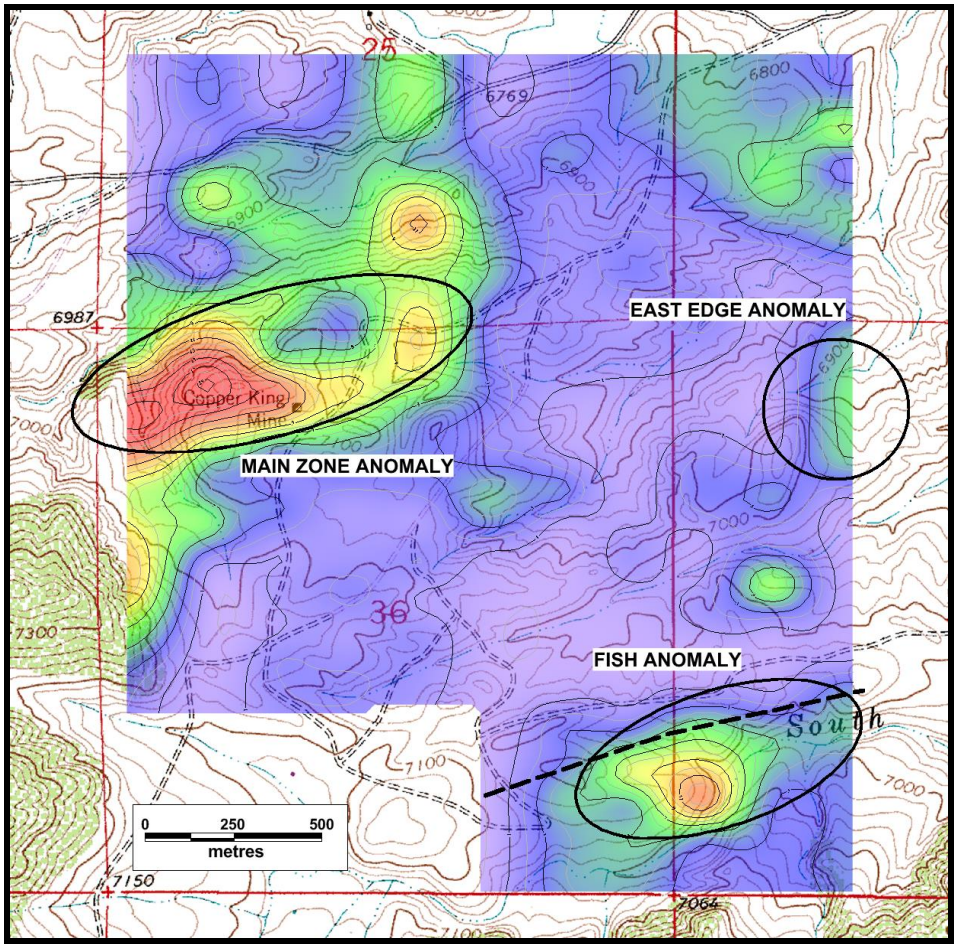

FIGURE 8: Chargeability 50 – 100 m Depth Slice over Topography

Three areas of anomalous chargeability are labeled on Figure 8. These include the main zone area with extensions to both the east and west from historic mine workings. The Fish anomaly, which is bounded by the aforementioned east-northeast structure along the north side and the east edge anomaly detected at depth on the eastern two lines.

DRILL PROPOSAL

As noted previously, the known mineralization correlates closely with coincident magnetic and chargeability anomalies. Clearly, other anomalies with coincidence between the two surveys should be considered priority targets. **However, strong anomalies in just one of the two parameters should not be excluded from consideration.** Figures 9 and 10 present four proposed drill holes over the magnetic and chargeability results.

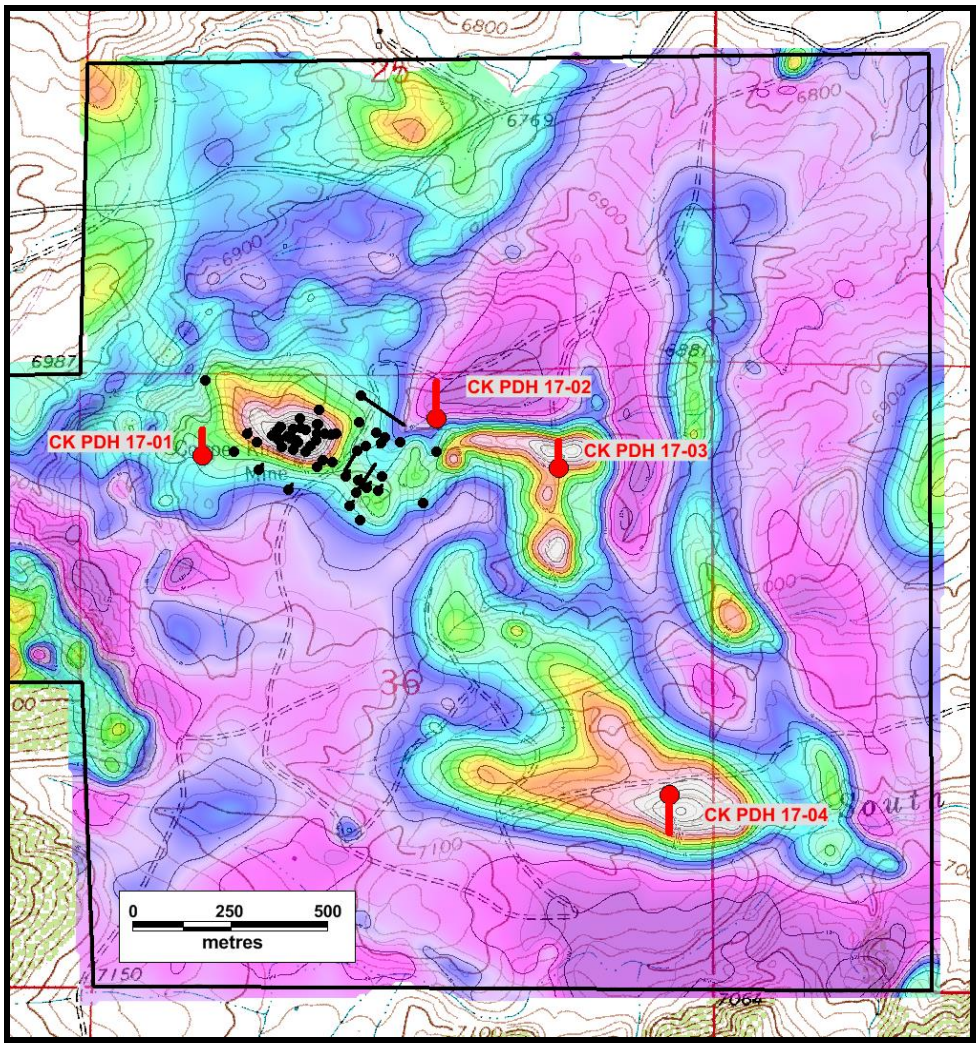

FIGURE 9: Residual RTP Magnetics, Proposed (●) and Historic (●) Drill Holes over Topography

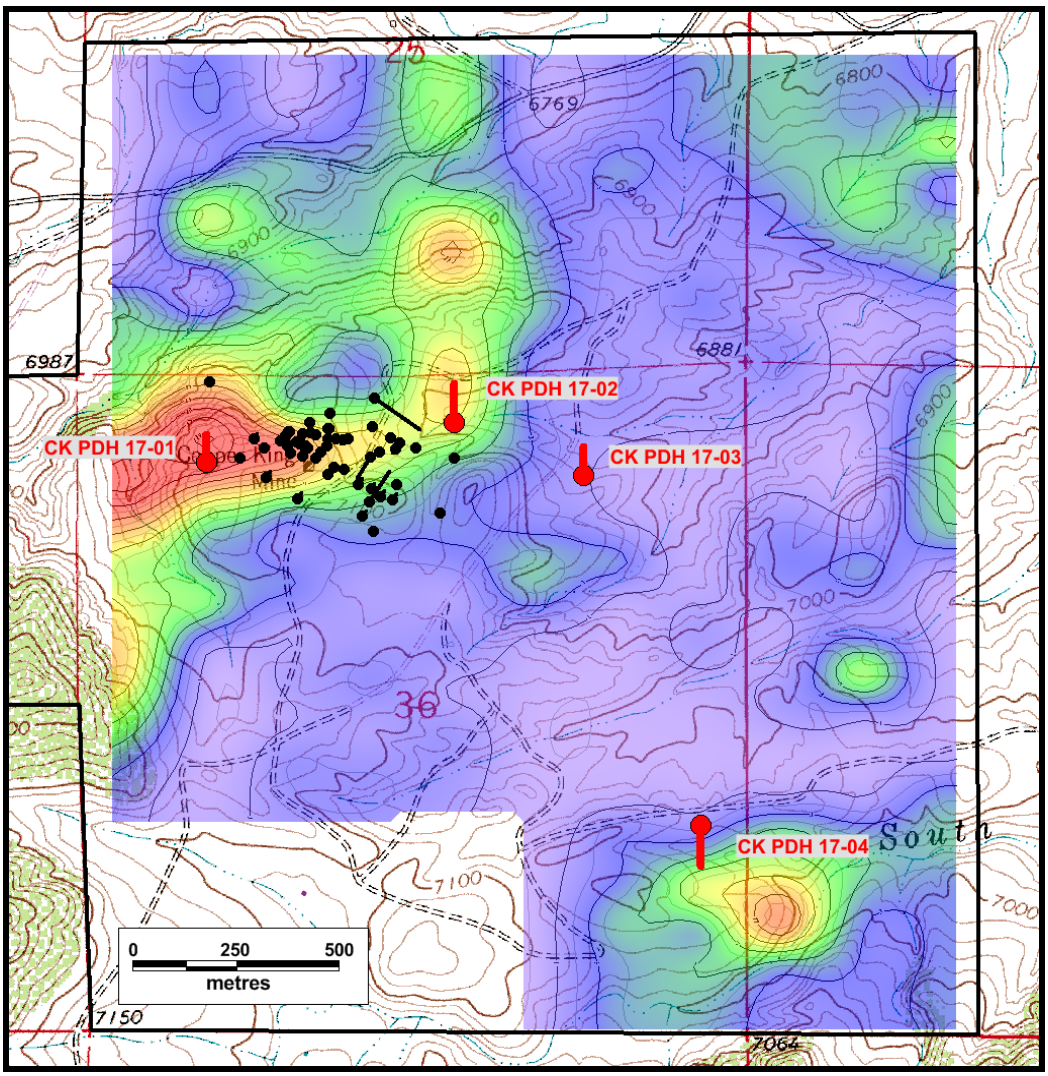

FIGURE 10: Chargeability 50 – 100 m Depth Slice, Proposed (●) and Historic (●) Drill Holes over Topography

The four proposed holes test coincident magnetic / chargeability anomalies along strike of known mineralization, as well as prominent magnetic responses. Holes CK PDH 17-01 and CK PDH 17-02 test moderate strength chargeability responses to the west and east of the main zone. As Figure 10 demonstrates, these appear to be extensions of the IP anomaly associated with mineralization. Hole CK PDH 17-03 targets a prominent magnetic anomaly which appears to be an easterly strike extension of the strong magnetic response associated with the main zone mineralization. Finally, hole CK PDH 17-04 targets the strongest magnetic response along the Fish anomaly with a proximal chargeability response. All holes are inclined 70° and designed to cut the target response at depth with sufficient length to assure crossing the source of the anomaly. Details concerning the proposed hole locations and geometry are provided in Table 1. Coordinates are **NAD 27 / UTM 13N**.

HOLE	COLLAR_E	COLLAR_N	TD (m)	AZIMUTH	INCL
CK PDH 17-01	484150	4554620	200	0	-70
CK PDH 17-02	484755	4554715	300	0	-70
CK PDH 17-03	485070	4554585	200	0	-70
CK PDH 17-04	485350	4553740	300	180	-70

TABLE 1: Proposed Drill Hole Details

CONCLUSIONS AND RECOMMENDATIONS

The induced polarization survey confirmed a moderate strength chargeability anomaly correlates directly with known copper mineralization and revealed possible extensions to mineralization both to the east and west. In addition, two other anomalous zones were detected to the southeast and east of the Copper King mine (see Figure 8). These two zones exhibit direct or proximal magnetic correlations similar to that at the main zone. A large area of possible alteration north of the mine is indicated by the resistivity as well.

Four (4) drill holes are proposed to test three of the chargeability anomalies and one of the magnetic anomalies. No additional geophysical work is recommended until he proposed drill program is completed.

REFERENCES

Wright, J. L., 2017, Copper King, Ground magnetic survey, GIS database: U. S. Gold Corporation company report.

APPENDIX A

IP/RESISTIVITY SURVEY
COPPER KING PROJECT

Laramie County, Wyoming

DATA ACQUISITION REPORT

Prepared for:

U.S. Gold Corporation
November 4, 2017
Zonge Job # 17053

INTRODUCTION

Zonge International, Inc. performed an IP/resistivity survey on the Copper King Project, located in Laramie County, Wyoming, for U.S. Gold Corporation. The survey was conducted during the period of 13-30 October 2017.

Marco Zamudio, Geophysical Crew Chief for Zonge International conducted survey operations under Zonge job number 17053. This report covers data acquisition, instrumentation and processing. Digital data files were provided to client representative, James L. Wright of Wright Geophysics, for quality control, plotting, modeling and interpretation.

A total of eleven lines were acquired using a standard 9-electrode dipole-dipole array with a dipole length (a-spacing) of 100 meters as designed by Wright Geophysics. Data were acquired in the time-domain mode using a 0.125 Hz, 50 percent duty-cycle transmitted waveform.

SURVEY DETAILS

Client	U.S. Gold Corporation	
Project Name	Copper King	
Project Number	Zonge Project# 17053	
Project Location	Laramie County, Wyoming	
Coordinate System	NAD 27, UTM Zone 13 North	
Acquisition Period	13-30 October 2017	
Personnel	Marco Zamudio	Crew Chief
	Kyle Richter	Field Technician
	Ryan Petrocco	Field Technician
	Ian Hancock	Field Technician
	James Vansandt	Field Technician
Number of Lines	11	
Total Line Coverage	16.2 line-kilometers	
Receiver Crews	1 receiver crew	
Transmitter Duty Cycle	Time-Domain 50%	
Frequency	0.125 Hz	
Array	Dipole-dipole	
Dipole Length	100 meters	
Equipment	Zonge GDP-3224 Receivers (Qty 1)	
	Zonge GGT-9 Transmitter (Qty 1)	
	Zonge ZMG-9 Motor Generator (Qty 1)	
	Zonge ZMG-30DL Motor Generator (Qty 1)	

DATA ACQUISITION

Data were acquired along eleven lines oriented north-south. Stations were located using a Garmin hand-held GPS, model GPSMAP 64CSx. The GPS data were differentially corrected

in real-time using WAAS corrections. Accuracy of the GPSMAP 60CSx typically ranges from 2-5 meters. Line control in the field utilized UTM Zone 13N NAD27 datum.

Data were acquired using a dipole-dipole electrode array with a dipole length (a-spacing) of 100 meters. Measurements were made for continuous line-coverage at n-spacing of 1 through 7.

Data were acquired in the time-domain mode using a 0.125 Hz, 50 percent duty-cycle transmitted waveform. Chargeability values (IPm) represent the Newmont Window with integration from 450 to 1100 milliseconds after transmitter turnoff. A discussion of the time-domain acquisition program is presented with the digital data release.

INSTRUMENTATION

Instrumentation consisted of a Zonge model GDP-3224 multiple purpose receiver, serial number 32258 The GDP-3224 is a backpack-portable, 24-bit, microprocessor-controlled receiver that can gather data on as many as eight channels simultaneously.

The electric-field signal was measured at the receiver site using non-polarizing ceramic porous-pot electrodes connected to the receiver with insulated 14-gauge wire.

The signal source for the IP measurements was a Zonge GGT-10 transmitter, serial number 558A. The GGT-10 is a constant-current 10 KVA transmitter. Power for the transmitter was provided by a Zonge ZMG-9, 9 KVA motor-generator with an external voltage regulator. The ZMG-9 alternator bearing started to fail on October 14th. A replacement Zonge ZMG-30DL motor-generator was mobilized to the project and arrived on October 16th. The Zonge ZMG-30DL motor-generator is 30 KVA generator which is equipped with a built-in voltage regulator. The transmitter was controlled by an XMT-G GPS transmitter controller, serial number 9EB5. Transmitter-receiver synchronization was maintained via GPS signal. Instrument specifications are included with the digital data release.

DATA QUALITY

The quality of an IP measurement is affected by extraneous electrical noise, as well as phenomena such as electromagnetic coupling (EM coupling), and coupling to man-made features (cultural coupling). At normal IP frequencies, telluric currents in the earth can be a significant problem, degrading the signal to noise ratio (S/N). Lightning discharges (sferics) from thunderstorm activity create electrical noise that degrades the data quality. These types of noise sources can degrade measurement repeatability. Both types of noise usually exhibit temporal variations. The S/N decreases for lower transmitted currents, larger n-spacing, and lower ground resistivity. The effects of these noise sources can be decreased by increasing the transmitted current and by stacking and averaging multiple cycles of the signal.

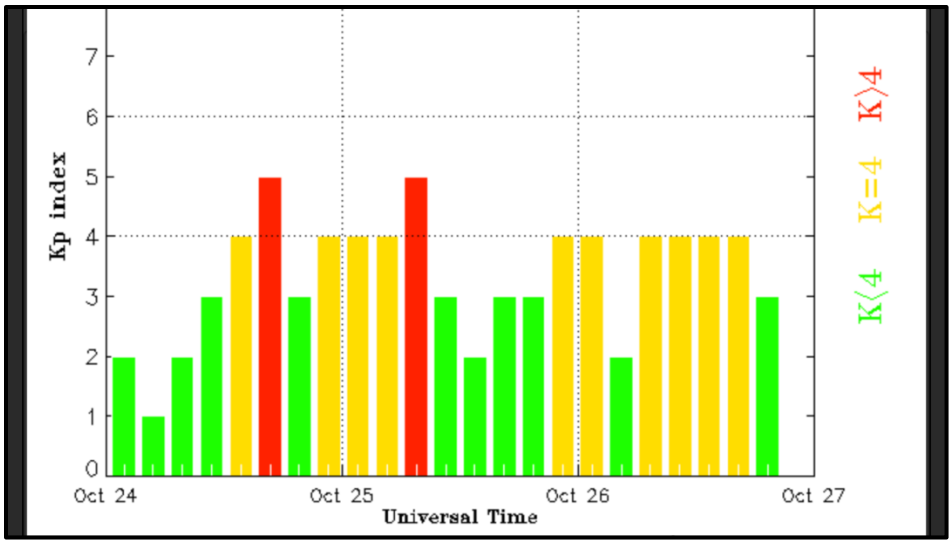

Figure 1: K-Index Chart

A moderate Geomagnetic storm was observed during the period of 10:30 to 13:30 local time on October 24th as seen in Figure 3. The telluric currents affected the IP data for 22 readings on line 485,350E. These readings were repeated on October 26th.

Noisy IP data were also encountered for 12 readings on line 485,150E on October 22nd. The noisy readings were thought to be caused by a decrease in S/N over an area of low resistivity. These readings were repeated on October 29th with no significant improvement to the data quality.

Electromagnetic and cultural coupling are dependent on the resistivity structure of the ground and the existence of manmade features, respectively. The effects are not reduced by increasing the transmitter signal or by stacking and averaging and do not affect the repeatability of the measurements.

The effects of extraneous electrical noise are evaluated by checking the difference between repeat measurements for the same data point. Typically, at least three measurements are made for each data point, and in high noise environments the total may be considerably more. The number of signal cycles that are stacked for each measurement is determined by the operator, based on whether the noise is caused by periodic or continuous noise. The difference in the values for multiple readings (repeatability) is a fundamental indicator of data quality.

Standard-error values and repeatability of multiple cycles are monitored in real-time during acquisition. Spurious readings caused by sources such as distant lighting strikes can be identified and are rejected during acquisition. Multiple measurements (typically a minimum of 3) are saved. The repeatability of the data can be assessed by review of the .zdb files which show the individual stacks that were averaged.

The measurement repeatability for dipole-dipole arrays can also be assessed by interchanging the transmitter and receiver dipoles. The principle of reciprocity provides that measurements

between two pairs of electrodes will be the same regardless of which pair is used as the transmitter or receiver. The standard 9-electrode spread used for this survey provides for reversed measurements at n= 4, 5 and 6 at the center of the spread. Since the signal to noise ratio decreases with increasing n-spacing, the differences at the greatest n-spacing for each overlap have been used to provide a practical evaluation of data quality for this survey.

Another quantitative evaluation of data quality is derived from the calculated IP error. IP error demonstrates the variance amongst a set of repeat measurements for a single point.IP error is calculated as a weighted standard deviation for a given point based on the formula:

$$IP\ error = \sqrt{\frac{\sum[(IPobs - IPavg)(IPwgt)]^2}{\sum(IPwgt)^2}}$$

Where IP*obs* is the individual IP measurement, IP*avg* is the averaged IP measurement, and IP*wgt* is the IP data weight for each individual measurement. Weighing methods are selectable as "straight" or "robust". Robust averaging will de-weight outliers and straight averaging will assign equal weight to each IP*obs*. Skipped IP*obs* measurements are assigned a weight of 1.0E-6 to minimize their effect on the averaging routine.

The calculated IP error values are provided in the LineNumber.dat file, provided on the digital data release, under column IPerr.

Data collected on this project are of moderate to good quality for data acquired from n=1 to n=7. Measurements in the field demonstrated moderate to good repeatability and IP error values are mostly less than 2 msec.

Culture encountered during the course of this project includes numerous fences, a power line and a buried water pipeline. Locations of the cultural features are plotted on the line location map and included in the digital date release as a CSV file for each line.

DATA PROCESSING

Routine data processing consists of the following steps:

1) The raw instrument files are reviewed to evaluate the data quality.
2) Spurious data which are obvious outliers with respect to multiple repeat measurements are flagged and removed from further processing.
3) The Raw data files (.CAC) are edited and averaged for each data point in the TDAVGW (version 1.16s) program and output in a column-based ASCII file (.avg), and a Geosoft ASCII file (.dat), with a single averaged value for chargeability and resistivity for each data point. Pseudo sections are generated at this step, and checked for reciprocity. Individual measurements making up each average are saved in .zdb files and can be re-edited and re-averaged at a later date.

All section plots are included as digital data files. Digital data files were delivered electronically. See the file named readme.pdf provided with the digital data release for a description of contents.

SAFETY AND ENVIRONMENTAL ISSUES

No health, safety incidents or accidents occurred during the course of this survey. No environmental damage was sustained as a result of the survey. Vehicle travel was kept to existing roads.

PRODUCTION LOG

Date	Notes
10/11/2017	Mobilized from Reno, Nevada to Evanston, Wyoming
10/12/2017	Mobilized from Evanston, Wyoming to Laramie, Wyoming
10/13/2017	Started data acquisition on line 483950E.
10/14/2017	Completed line 483950E. Started Data acquisition on line 484150E.
10/15/2017	Continued data acquisition on line 484150E. Motor generator down due to mechanical issues. Replacement on the way for 10/16 deployment.
10/16/2017	Surveyed lines ahead and built electrode pits for the next 3 lines.
10/17/2017	Completed Line 484150E. Started data acquisition on line 484350E.
10/18/2017	Completed line 484350E. Started data acquisition on line 484550E.
10/19/2017	Completed line 484550E. Started data acquisition on line 484750E.
10/20/2017	Completed line 484750E. Started data acquisition on line 484950E.
10/21/2017	Completed line 484950E.
10/22/2017	Started data acquisition on line 485150E.
10/23/2017	Completed line 485150E. Started data acquisition on line 485350E.
10/24/2017	Completed line on 485350E.
10/25/2017	Started data acquisition on line 485550E
10/26/2017	Completed line 485550E. Repeated 24 noisy readings on line 485350E.
10/27/2017	Started data acquisition on line 485750E.
10/28/2017	Repeated 12 noisy readings on line 485150E. Continued data acquisition on line 485750E. Spent time troubleshooting low signal high noise readings.
10/29/2017	Completed line 485750E. Started data acquisition on line 485950E.
10/30/2017	Completed line 485950E.
10/31/2017	Demobilized from Cheyenne, Wyoming to Elko, Nevada
11/1/2017	Demobilized from Elko, Nevada to Reno, Nevada

APPENDIX B

INVERSION SUMMARIES

LINES

483950E, 484150E, 484350E, 484550E, 484750E, 484950E
485150E, 485350E, 485550E, 485750E, 485950E

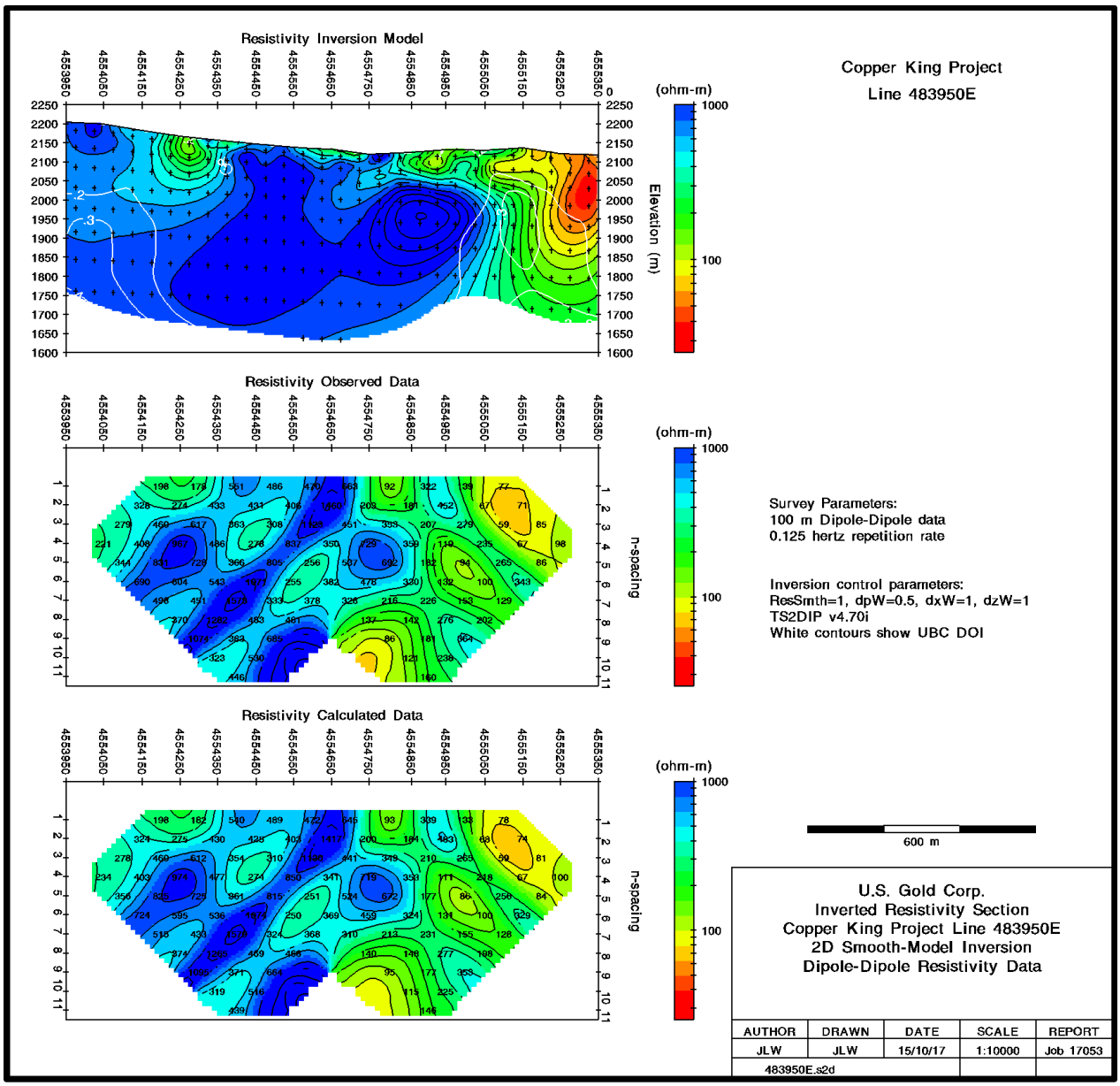

FIGURE 1A: Line 483950E Resistivity Inversion Summary

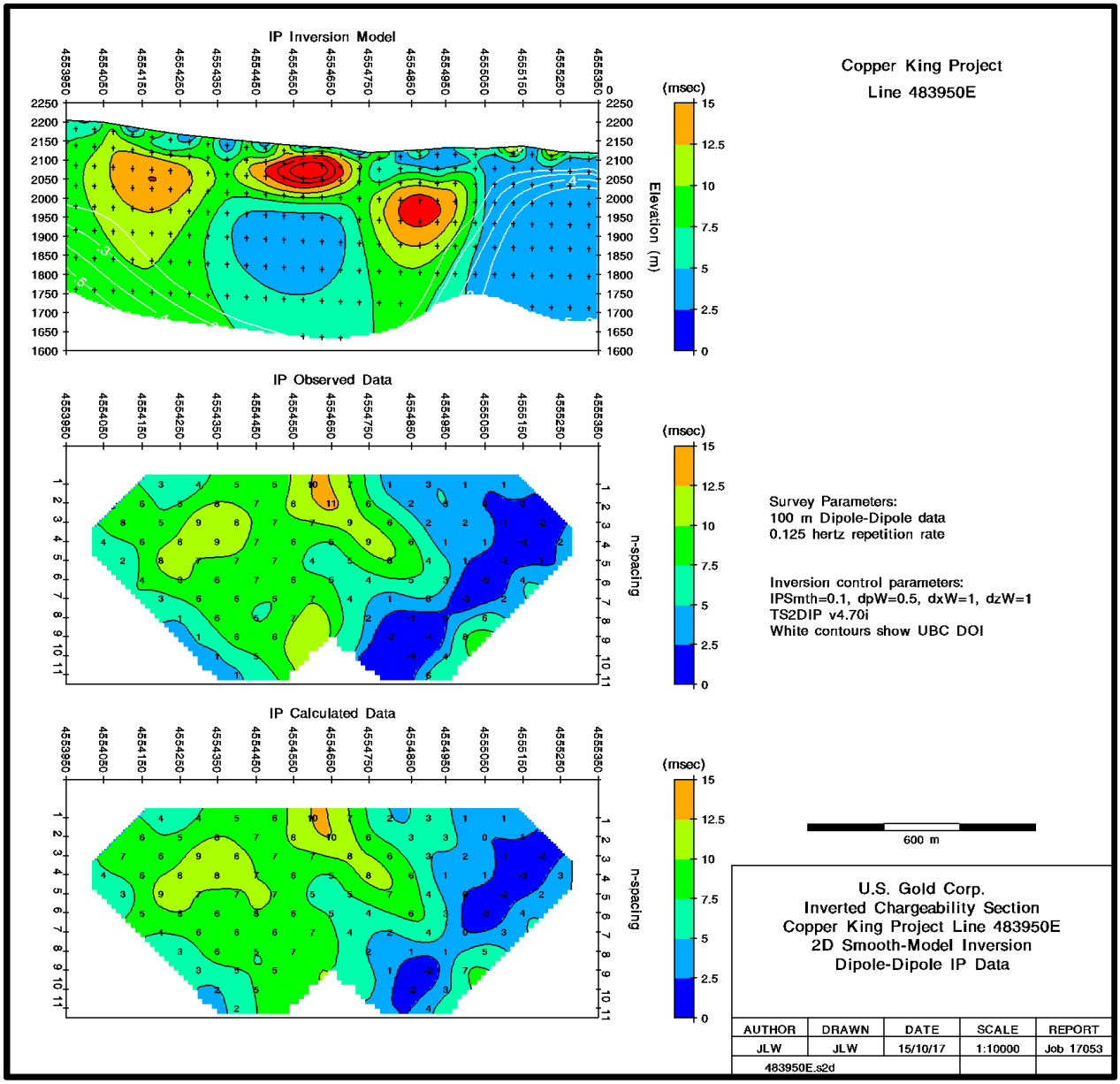

FIGURE 1B: Line 483950E Chargeability Inversion Summary

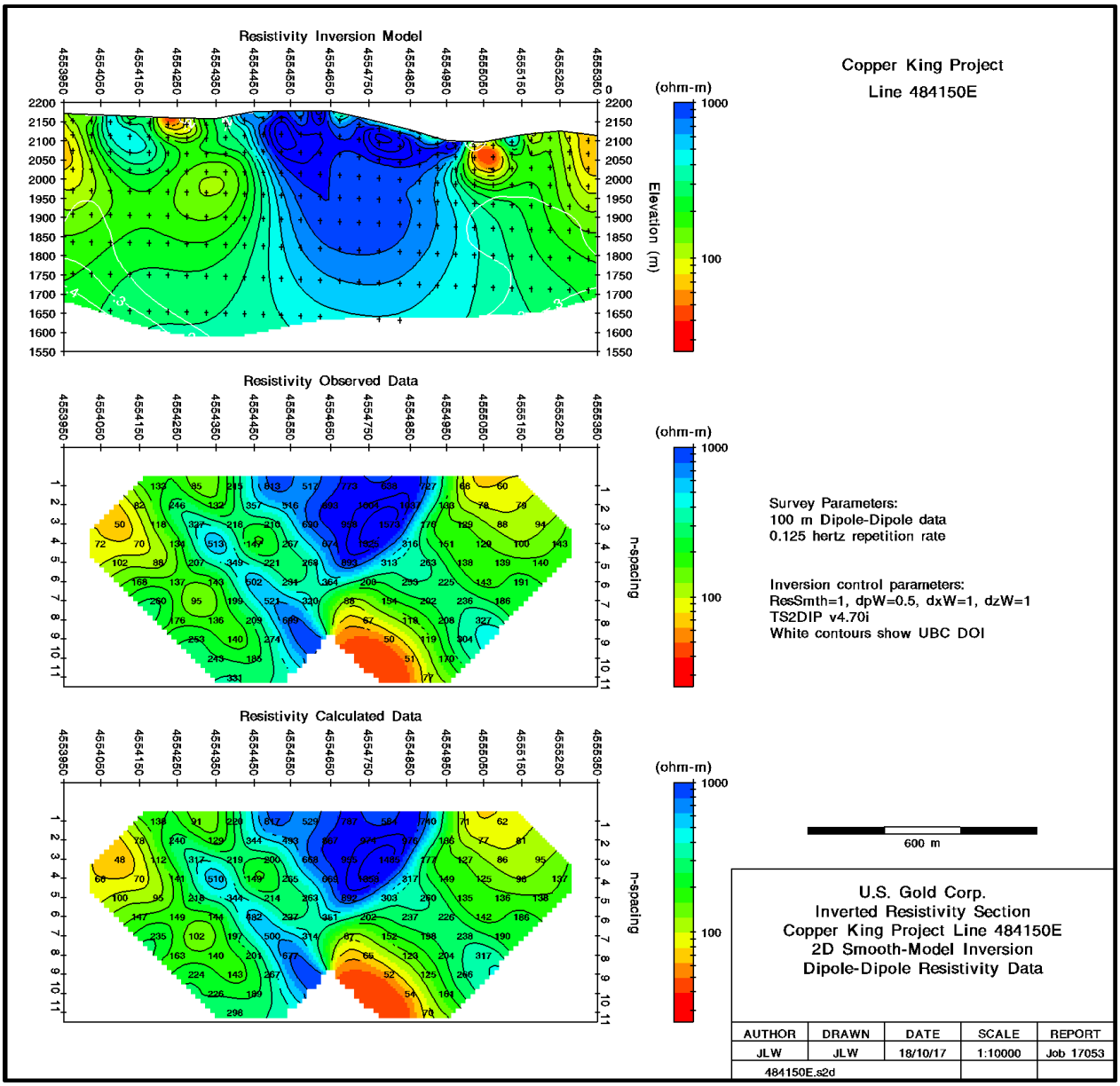

FIGURE 2A: Line 484150E Resistivity Inversion Summary

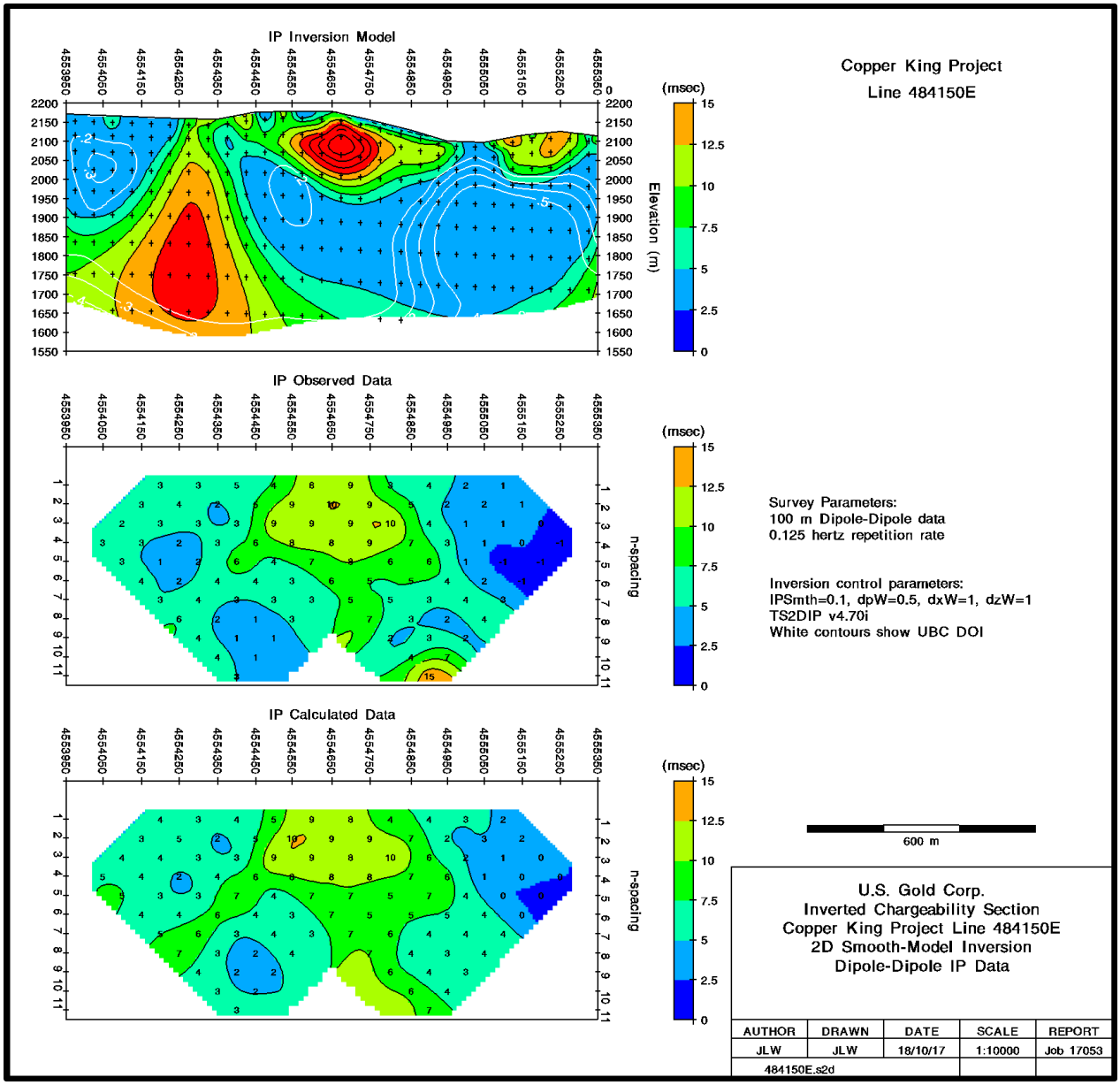

FIGURE 2B: Line 484150E Chargeability Inversion Summary

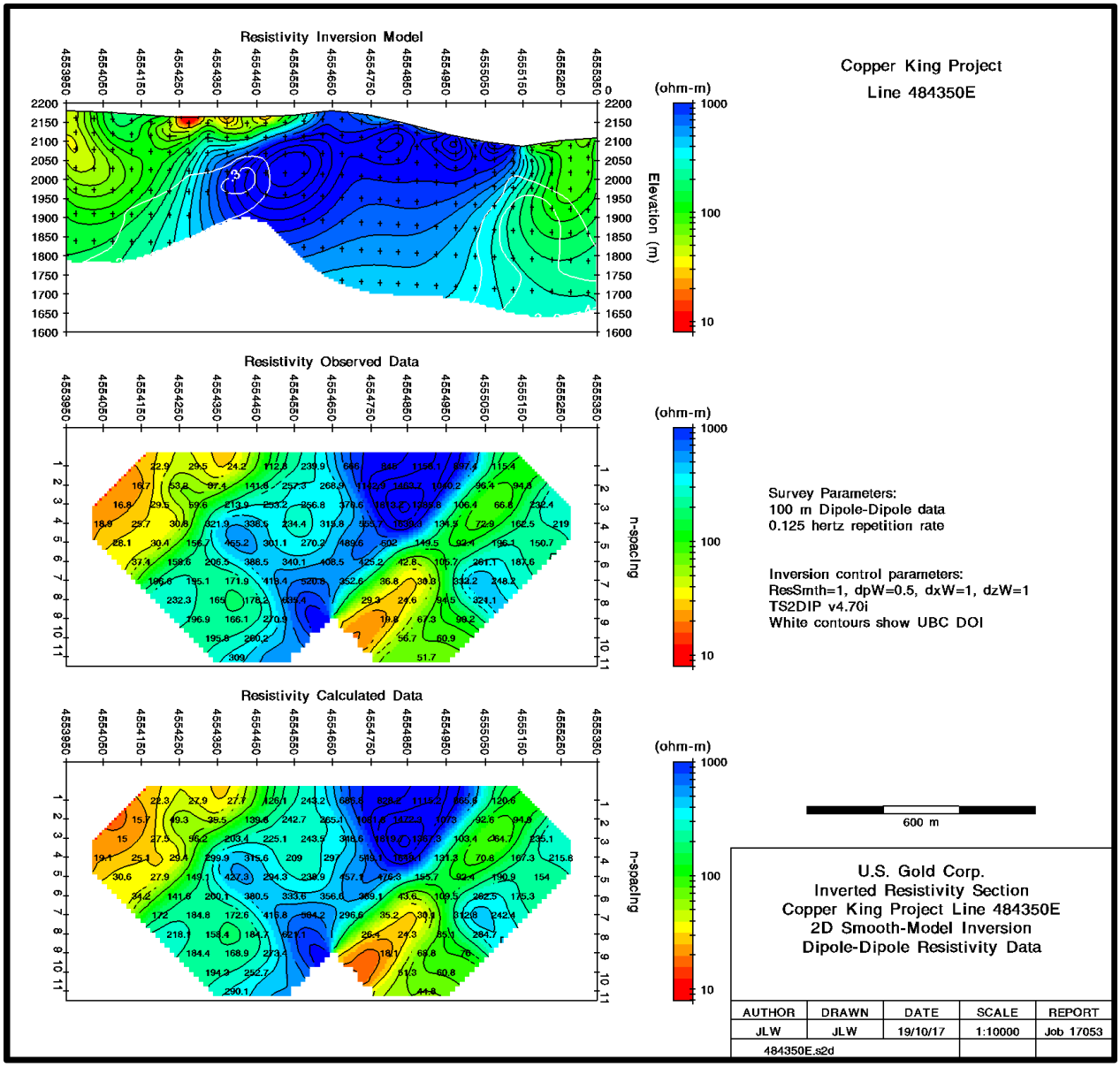

FIGURE 3A: Line 484350E Resistivity Inversion Summary

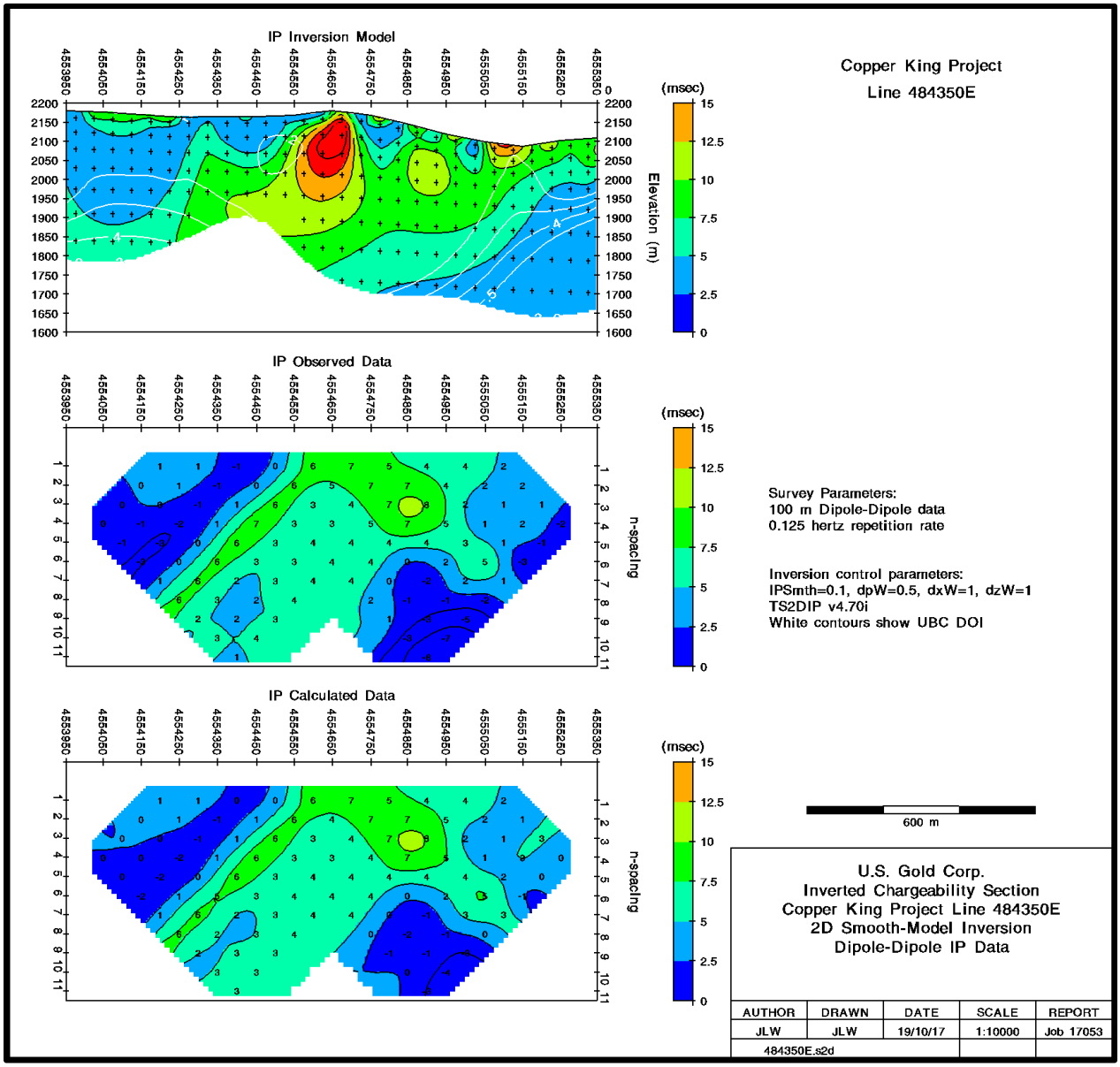

FIGURE 3B: Line 484350E Chargeability Inversion Summary

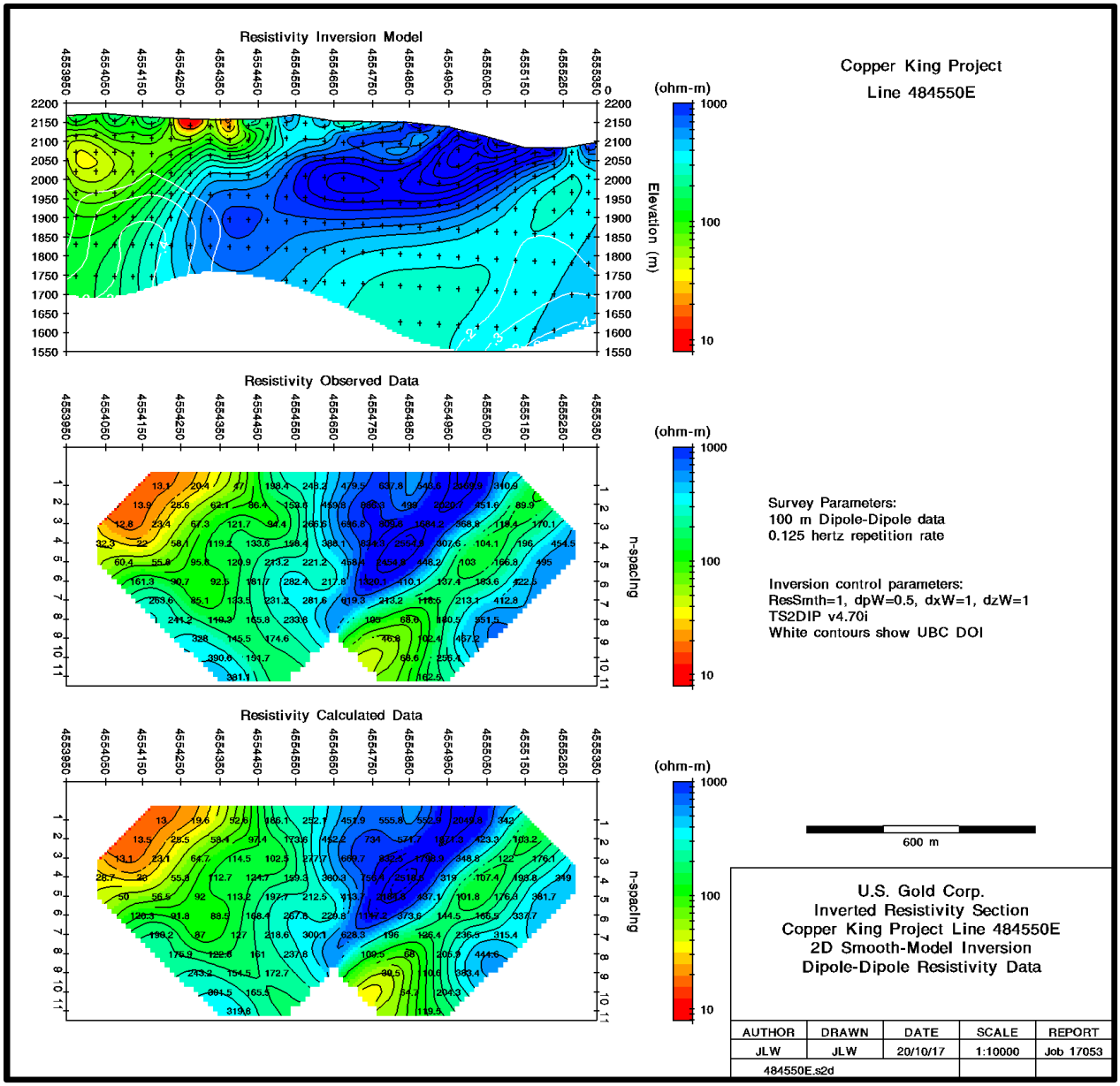

FIGURE 4A: Line 484550E Resistivity Inversion Summary

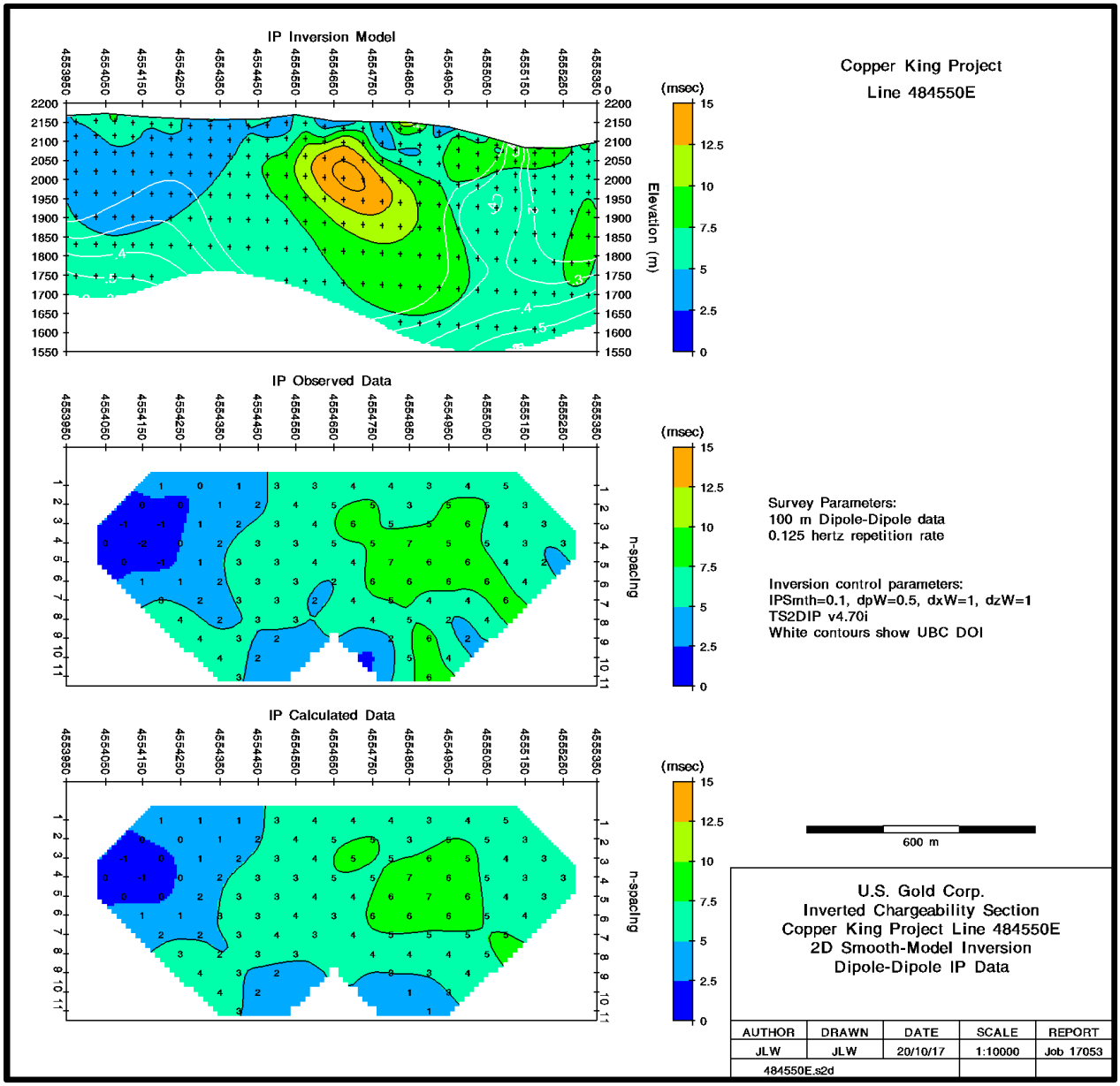

FIGURE 4B: Line 484550E Chargeability Inversion Summary

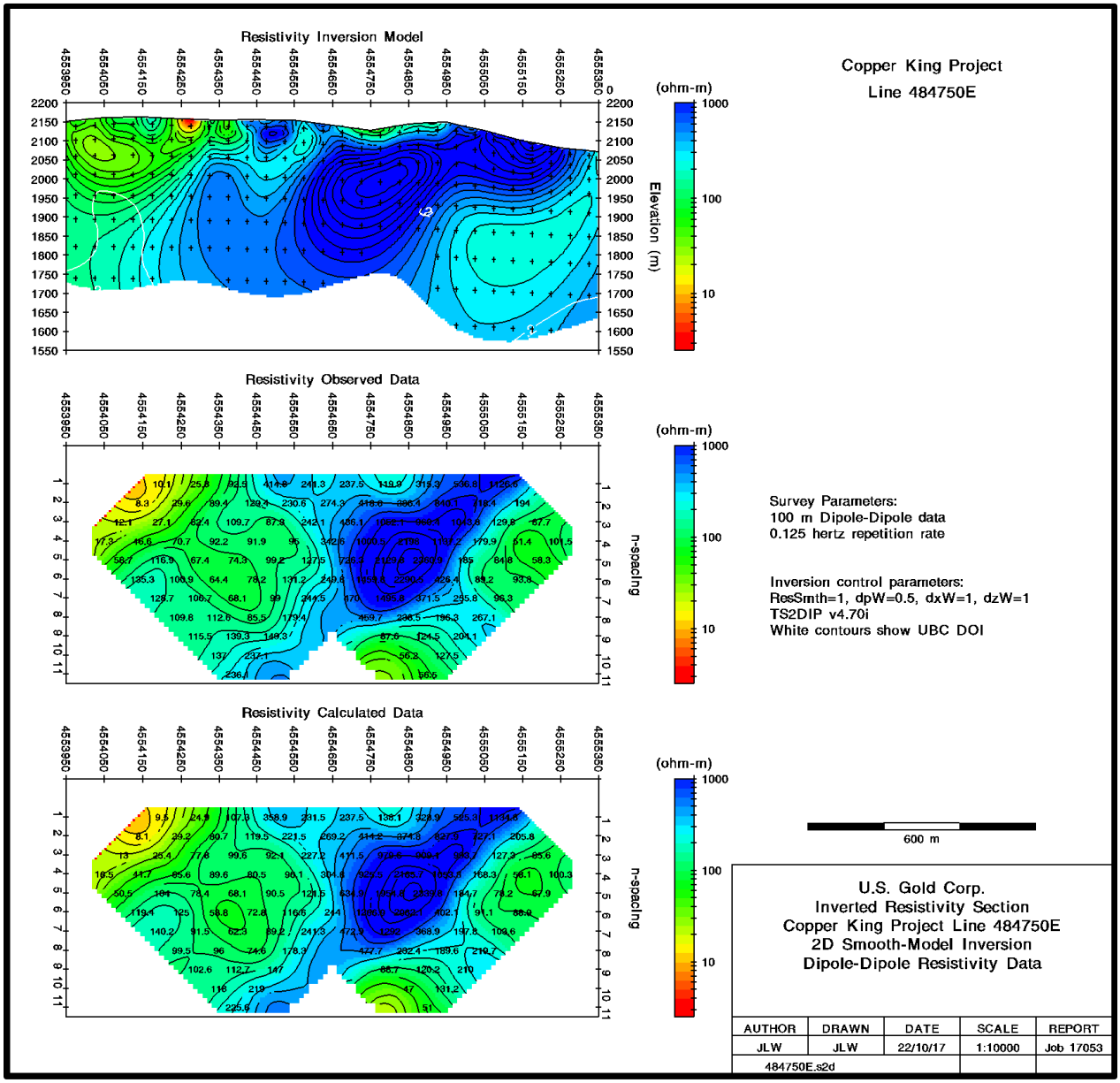

FIGURE 5A: Line 484750E Resistivity Inversion Summary

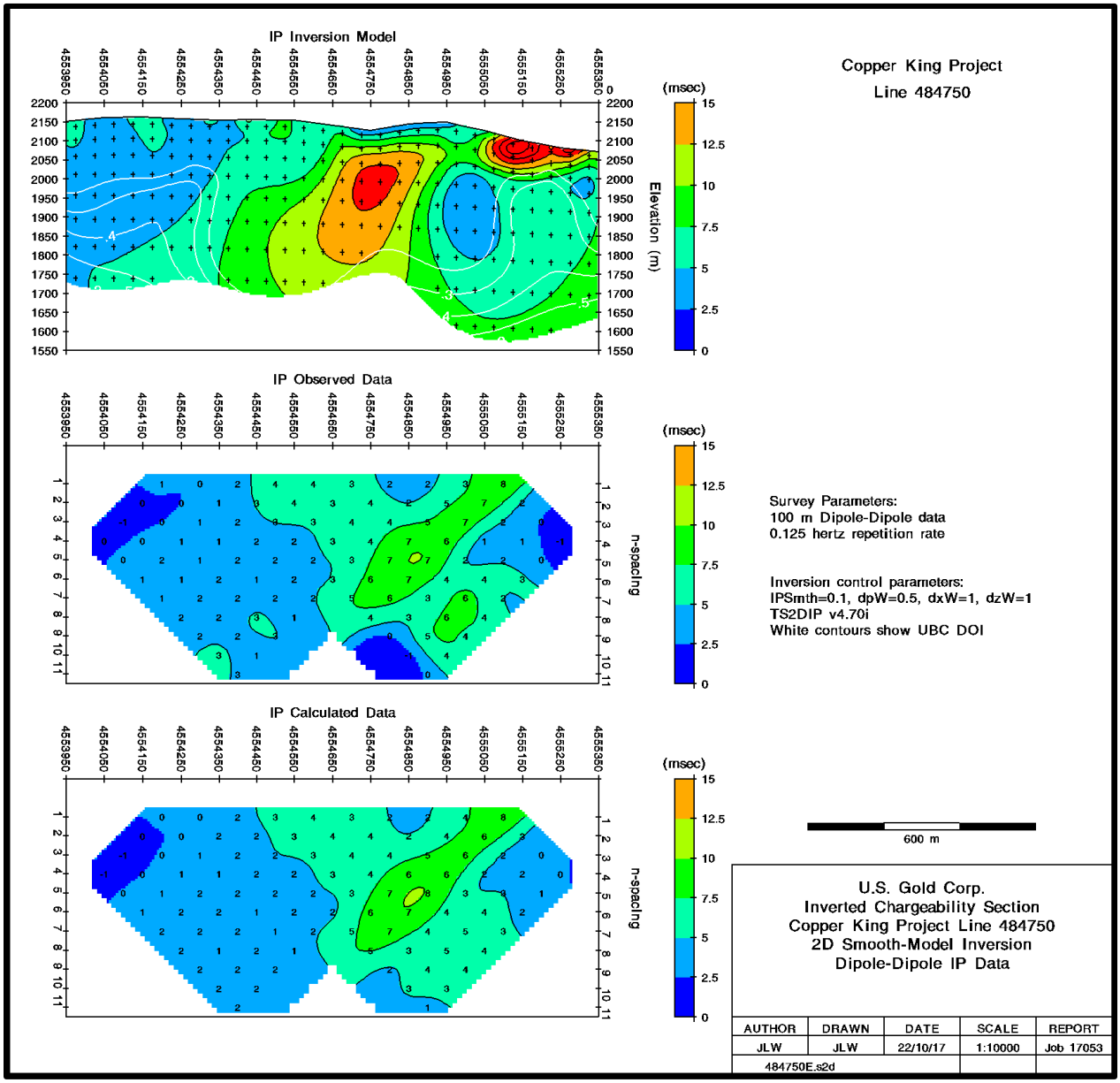

FIGURE 5B: Line 484750E Chargeability Inversion Summary

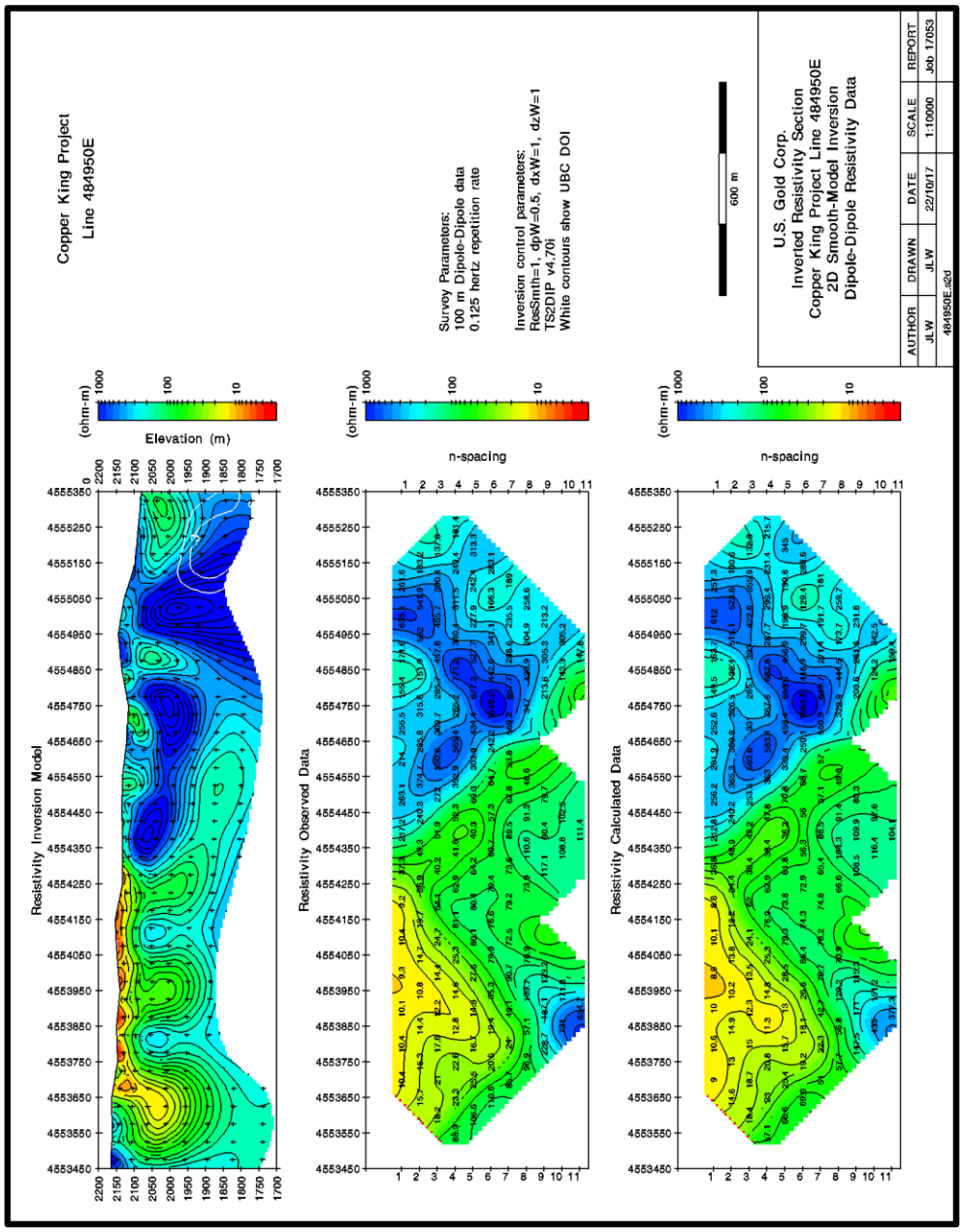

FIGURE 6A: Line 484950E Resistivity Inversion Summary

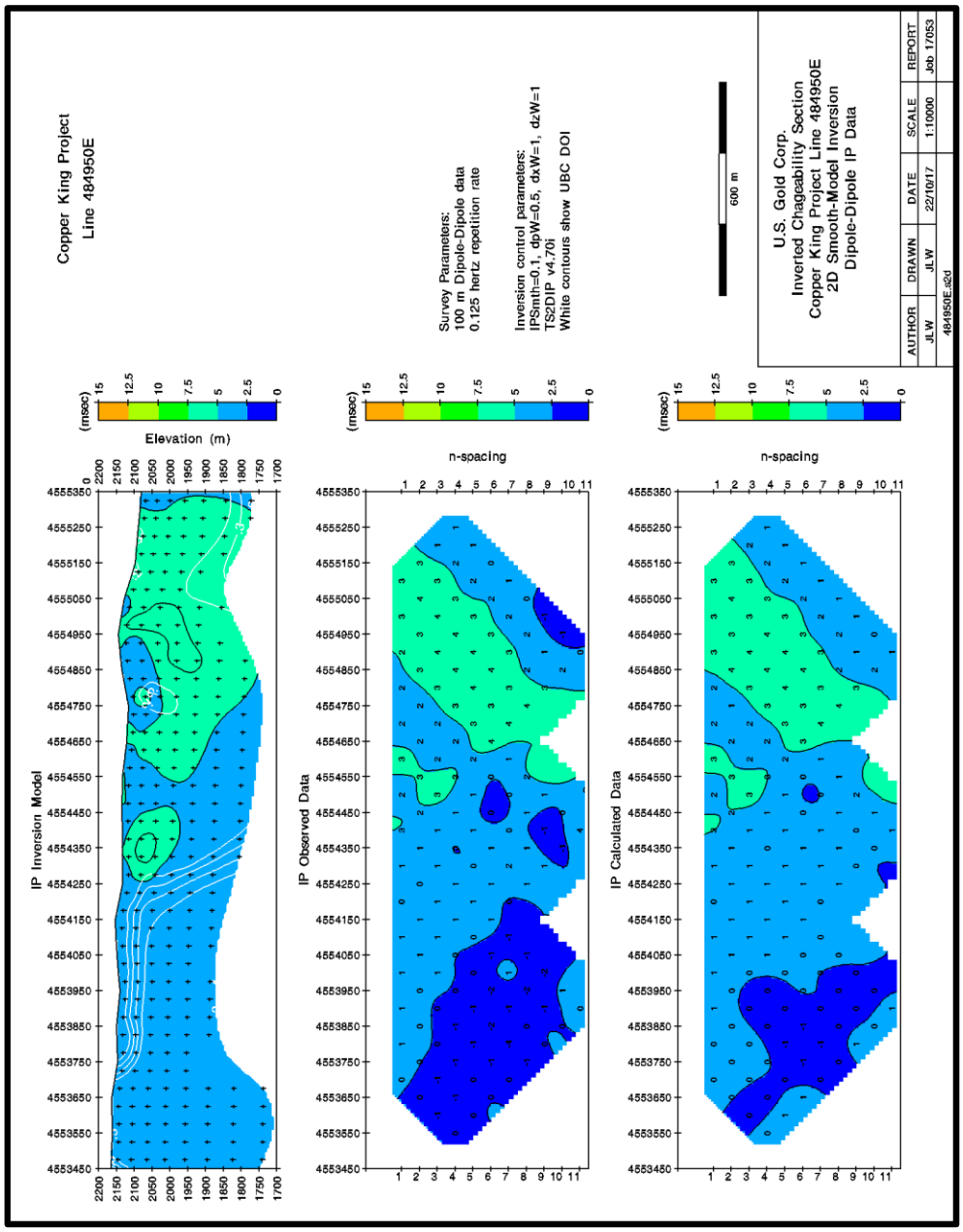

FIGURE 6B: Line 484950E Chargeability Inversion Summary

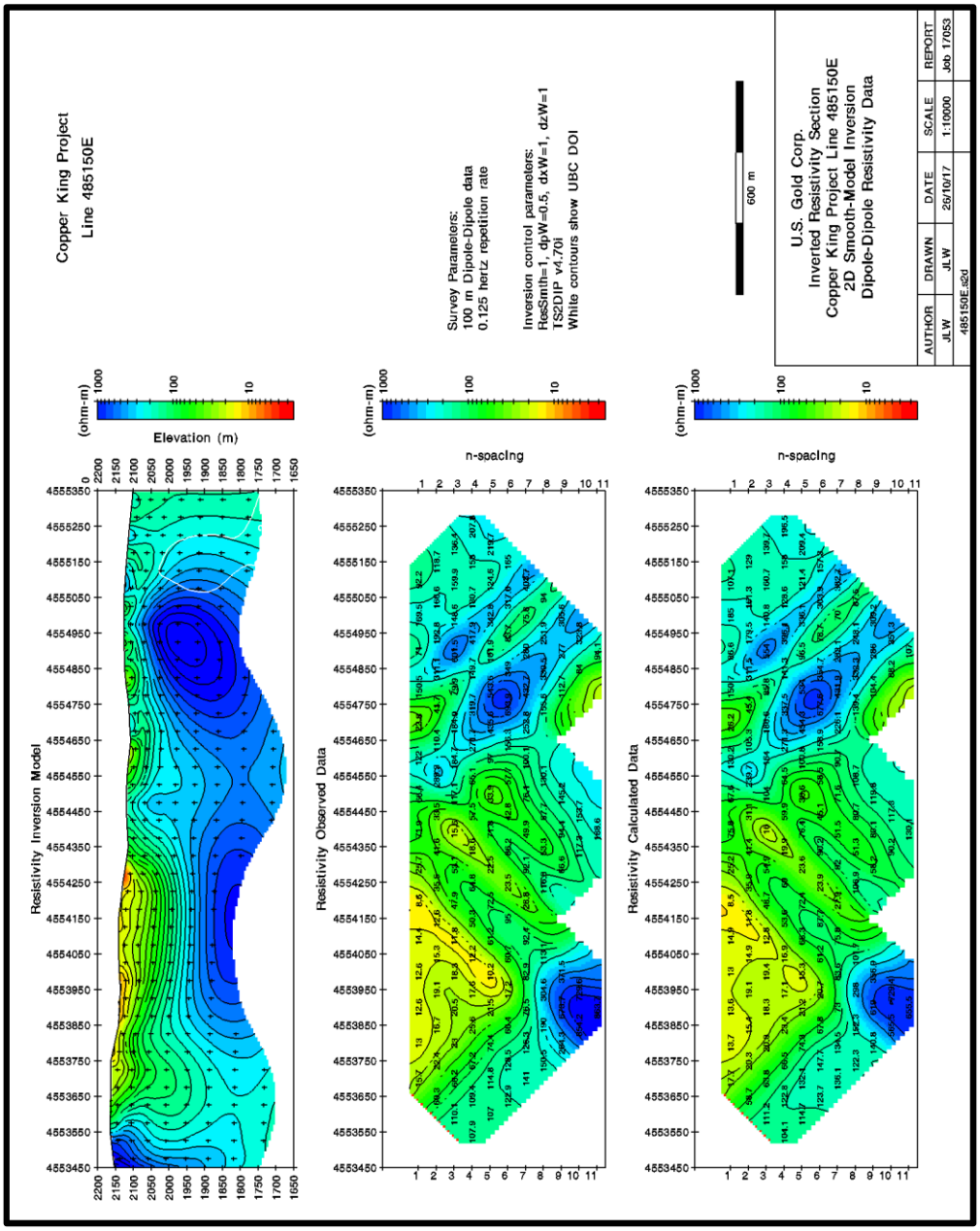

FIGURE 7A: Line 485150E Resistivity Inversion Summary

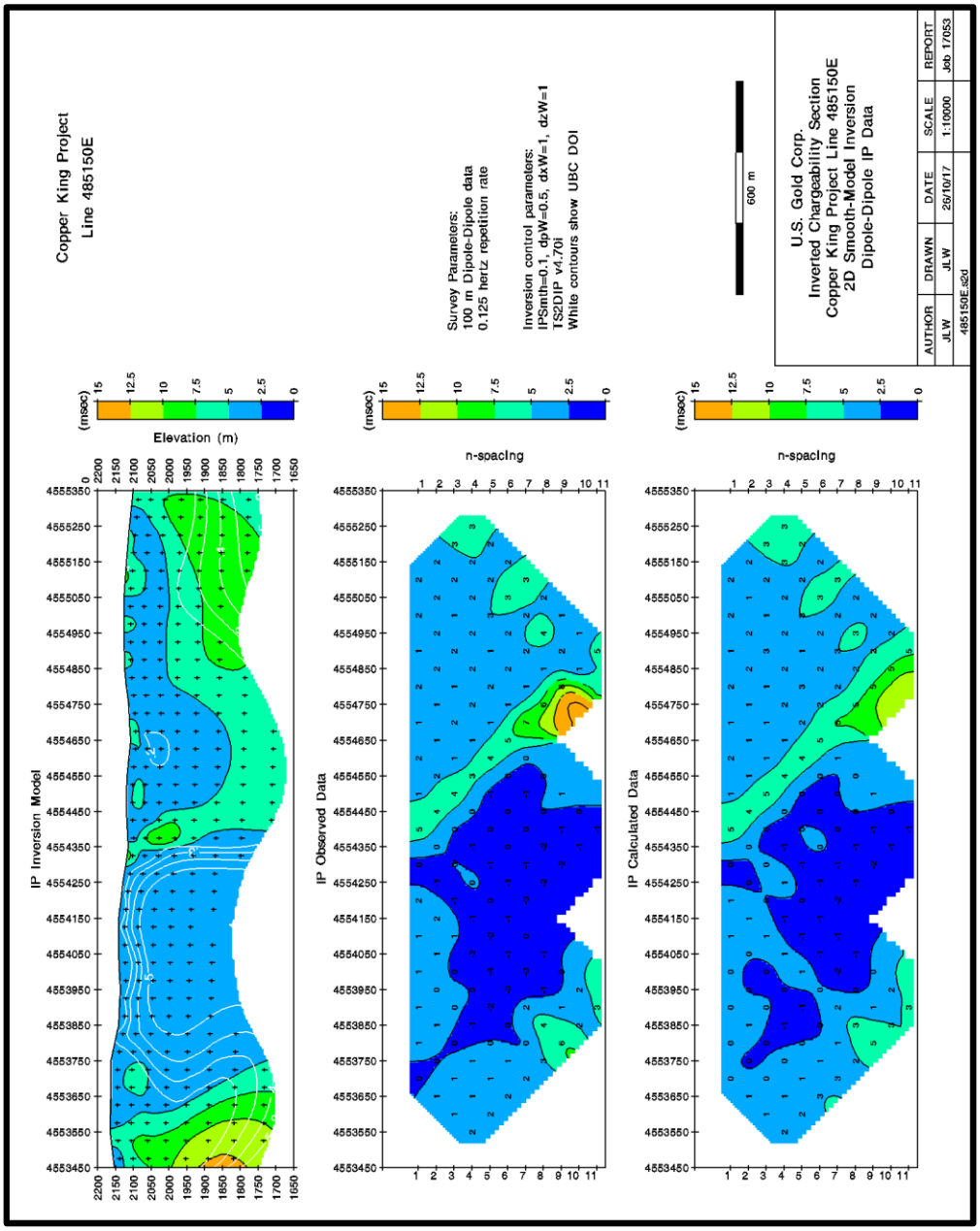

FIGURE 7B: Line 485150E Chargeability Inversion Summary

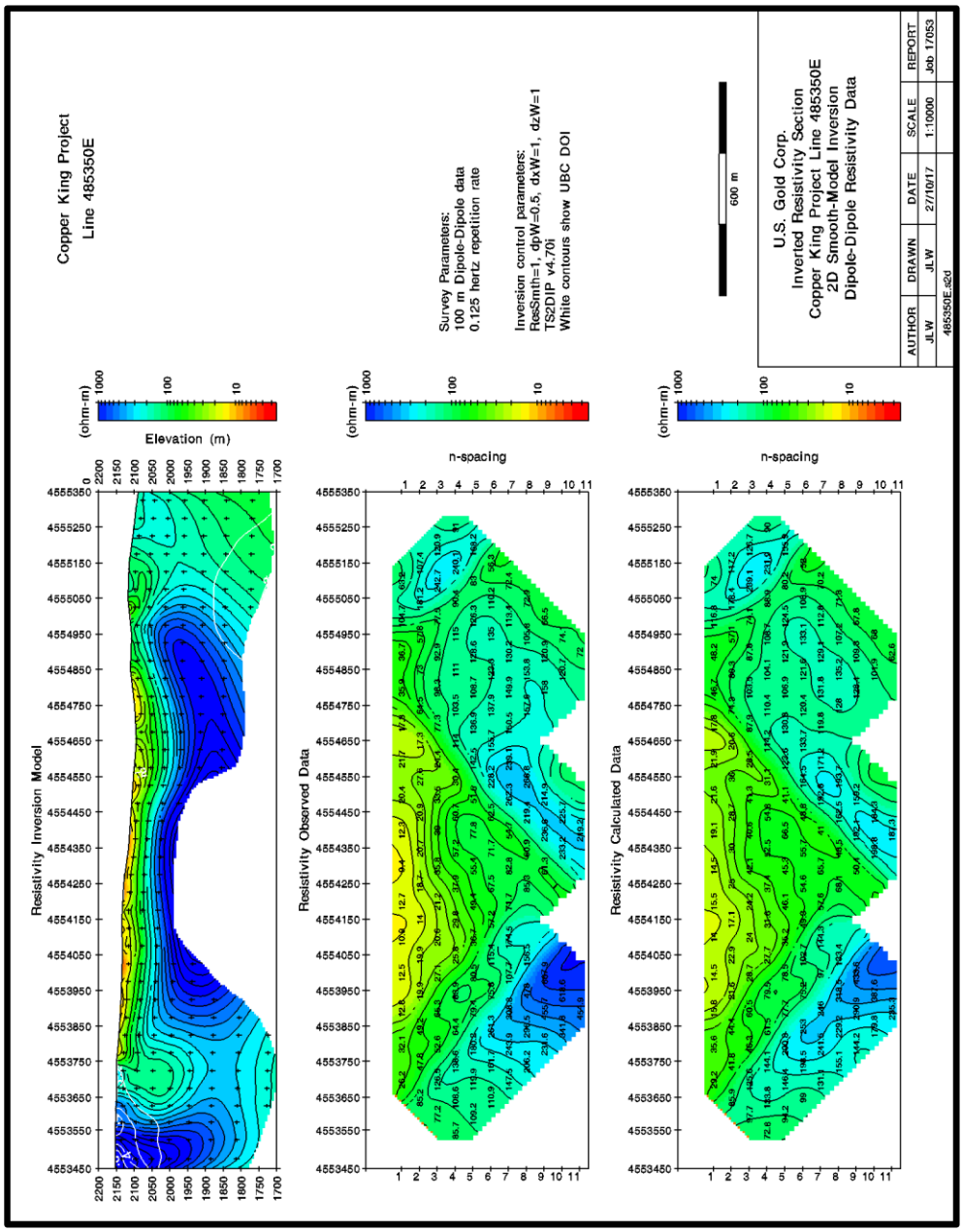

FIGURE 8A: Line 485350E Resistivity Inversion Summary

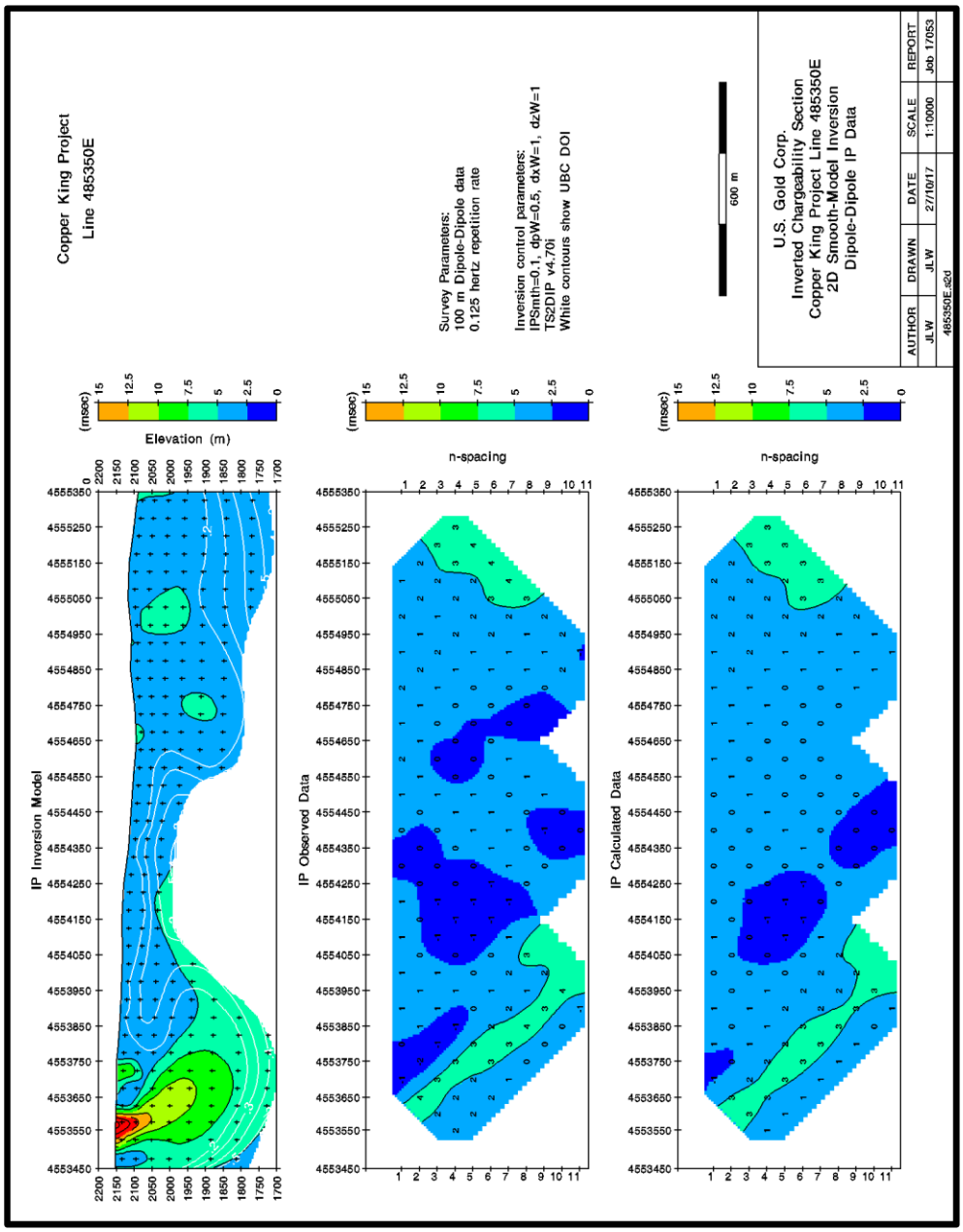

FIGURE 8B: Line 485350E Chargeability Inversion Summary

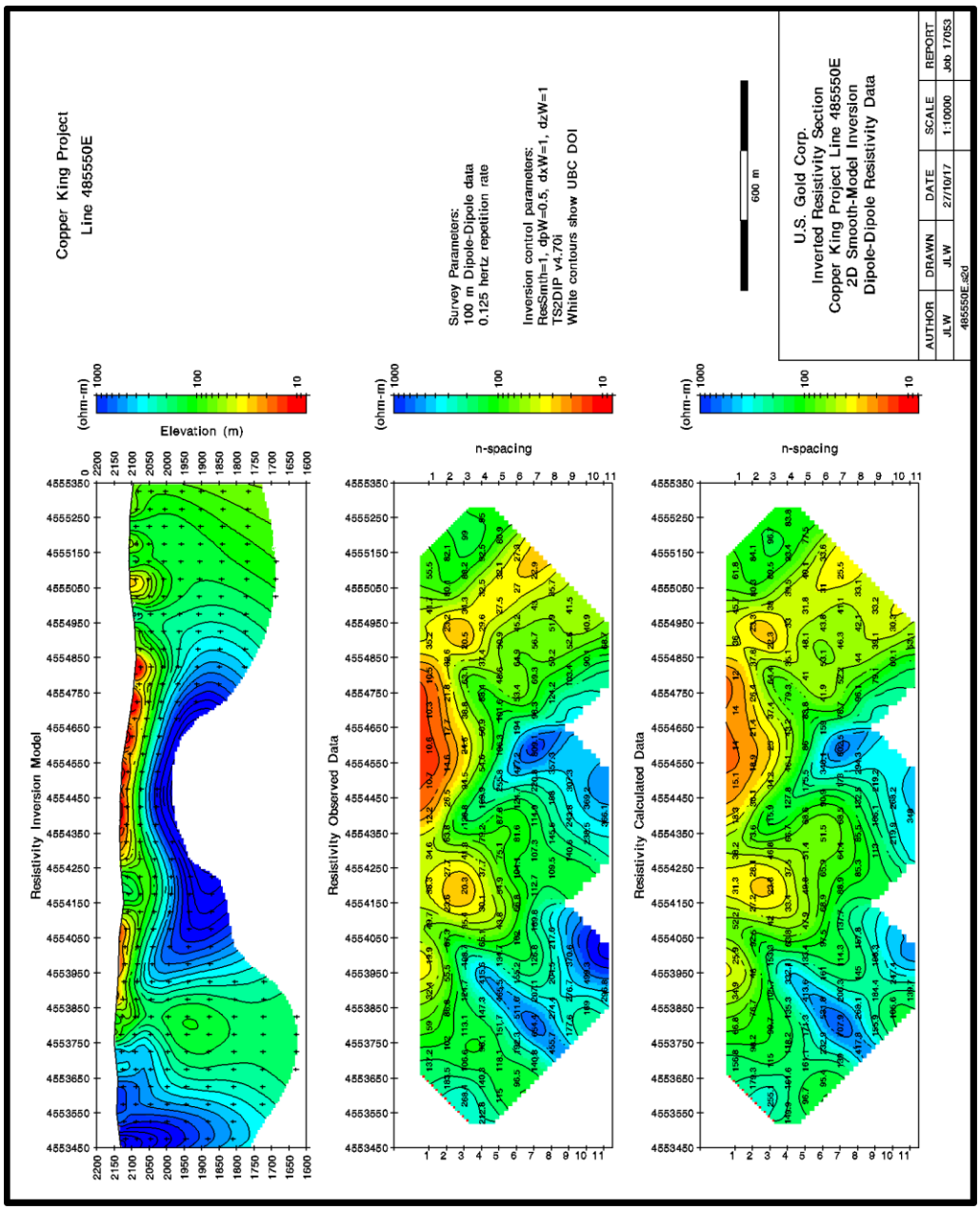

FIGURE 9A: Line 485550E Resistivity Inversion Summary

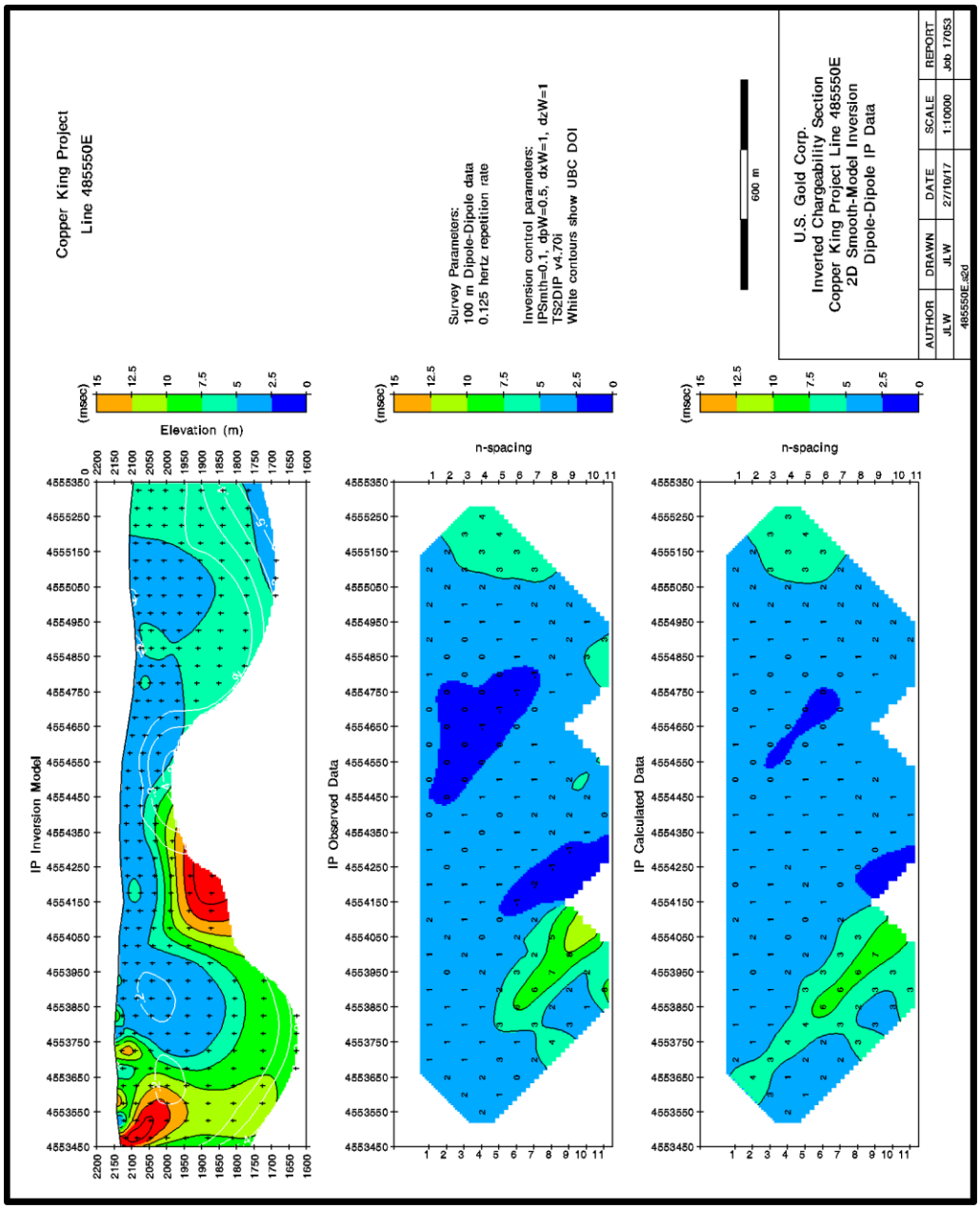

FIGURE 9B: Line 485550E Chargeability Inversion Summary

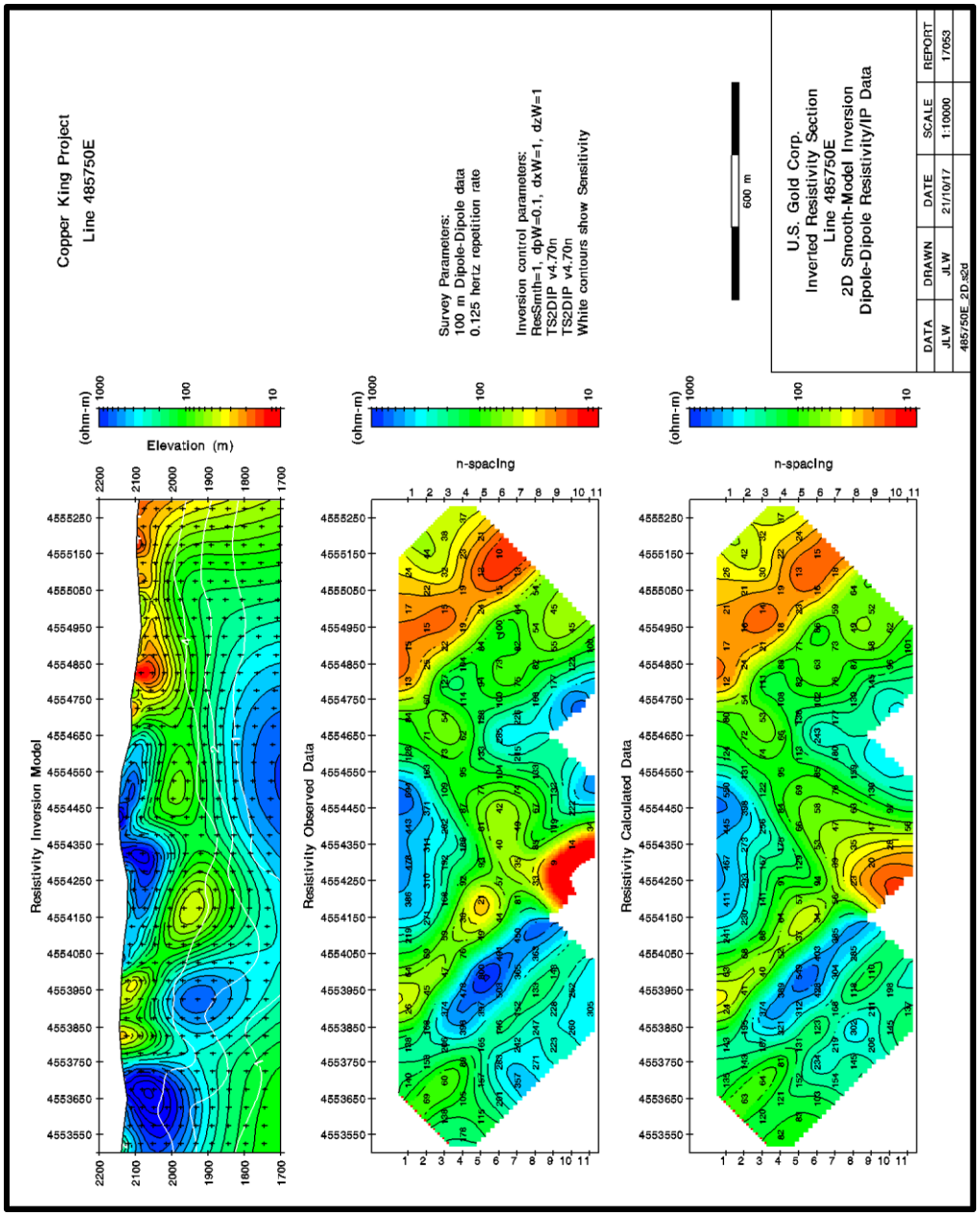

FIGURE 10A: Line 485750E Resistivity Inversion Summary

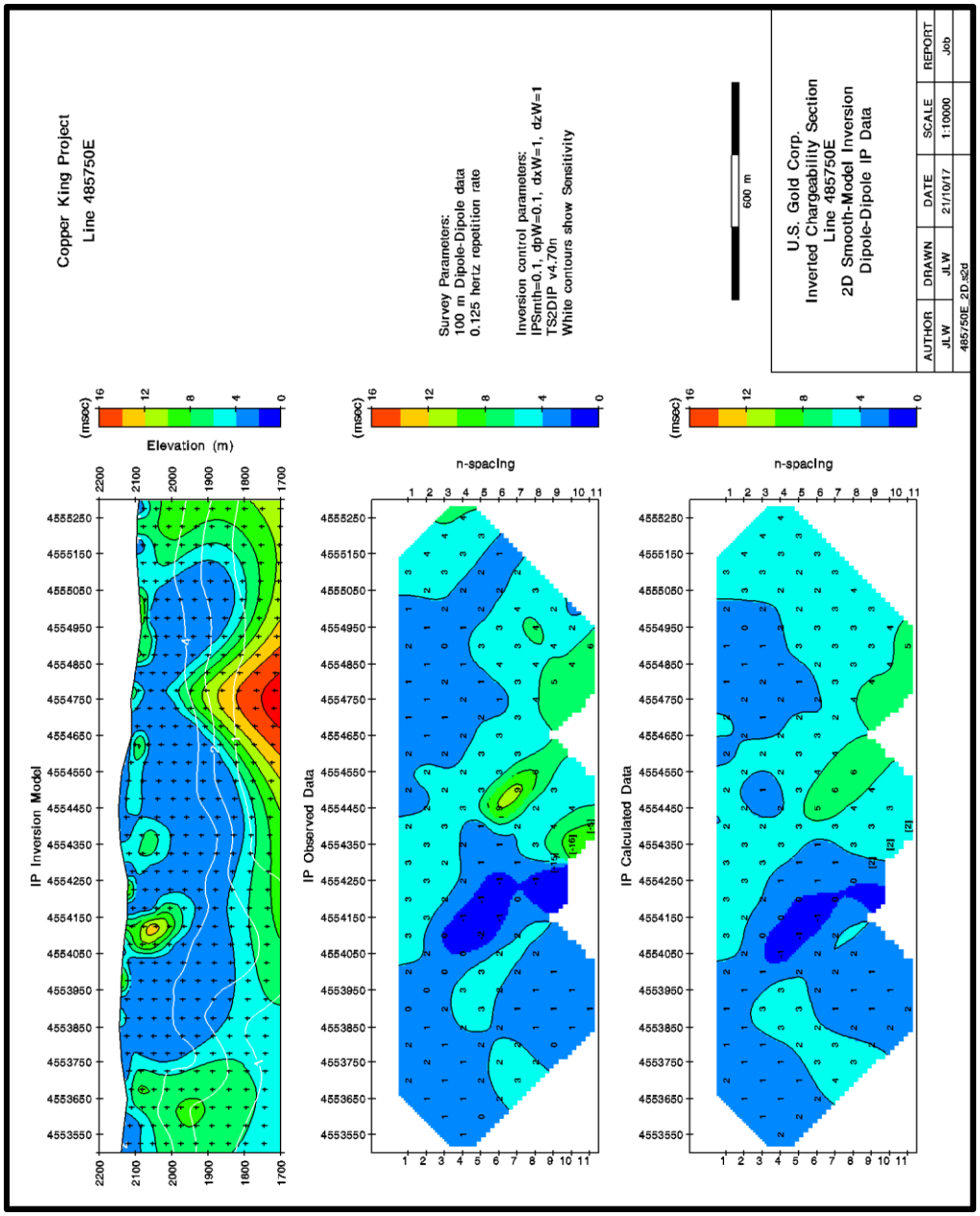

FIGURE 10B: Line 485750E Chargeability Inversion Summary

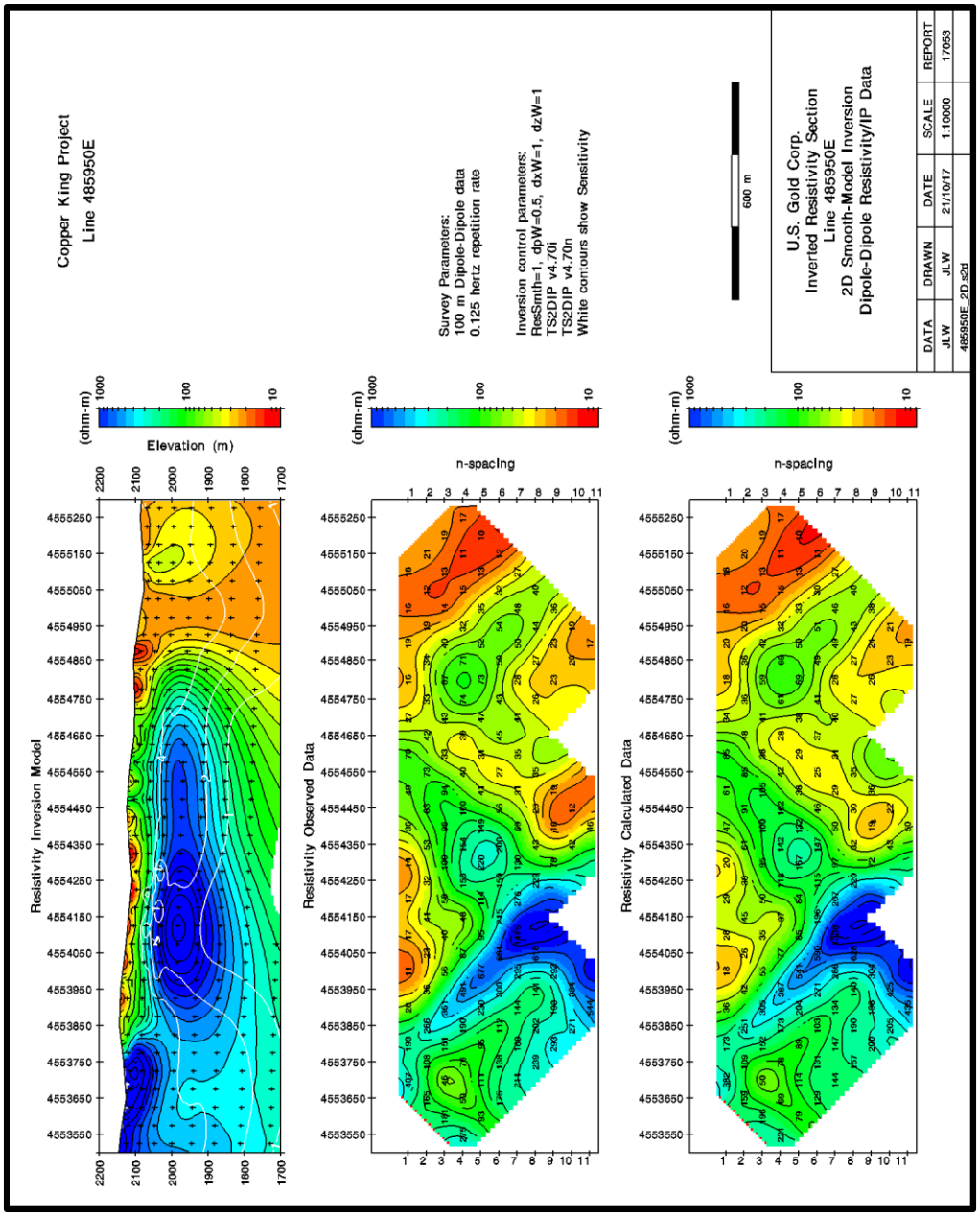

FIGURE 11A: Line 485950E Resistivity Inversion Summary

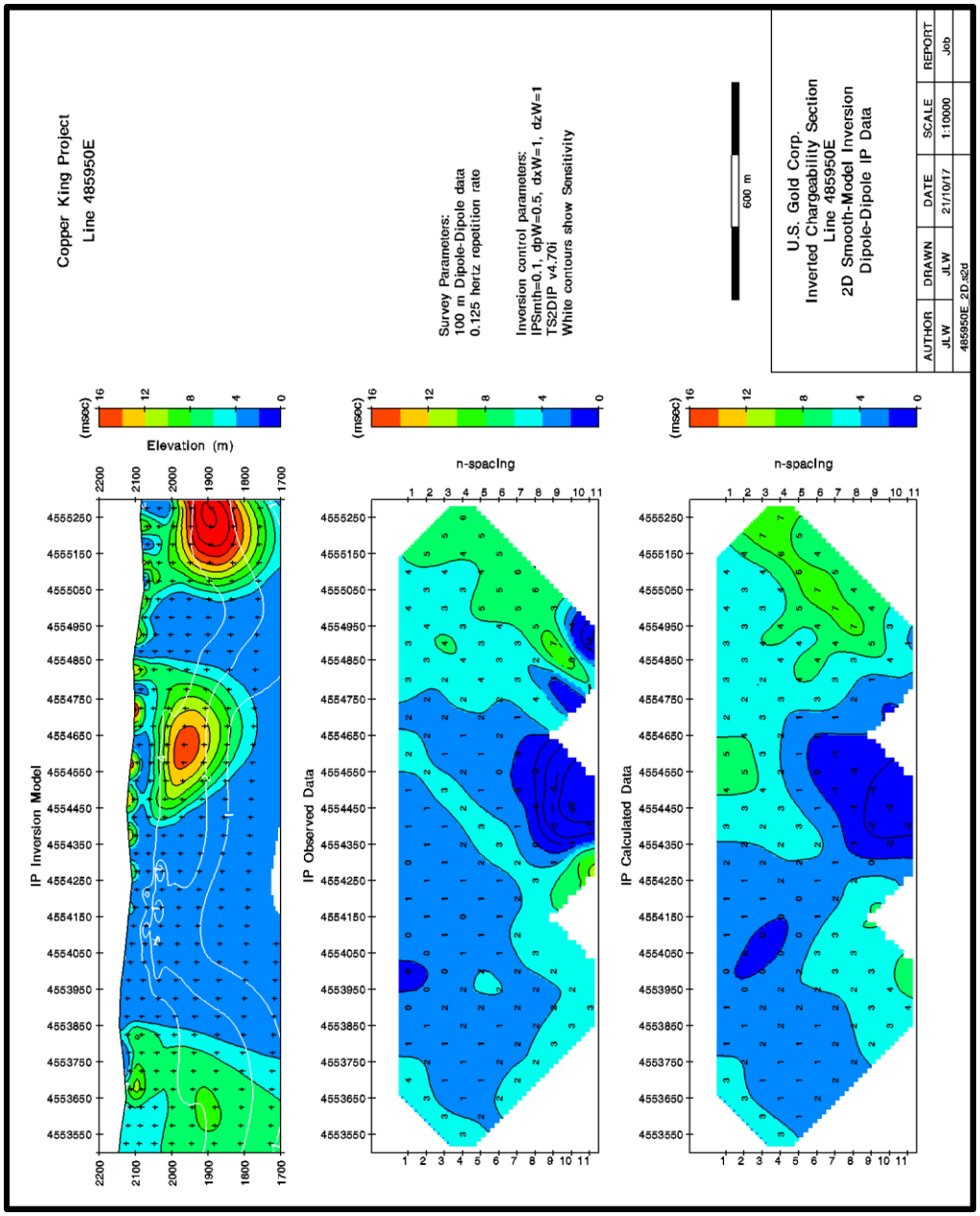

FIGURE 11B: Line 485950E Chargeability Inversion Summary

APPENDIX C

ROTATED TO PLAN IP SECTIONS OVER MAGNETICS

LINES

483950E, 484150E, 484350E, 484550E, 484750E, 484950E
485150E, 485350E, 485550E, 485750E, 485950E

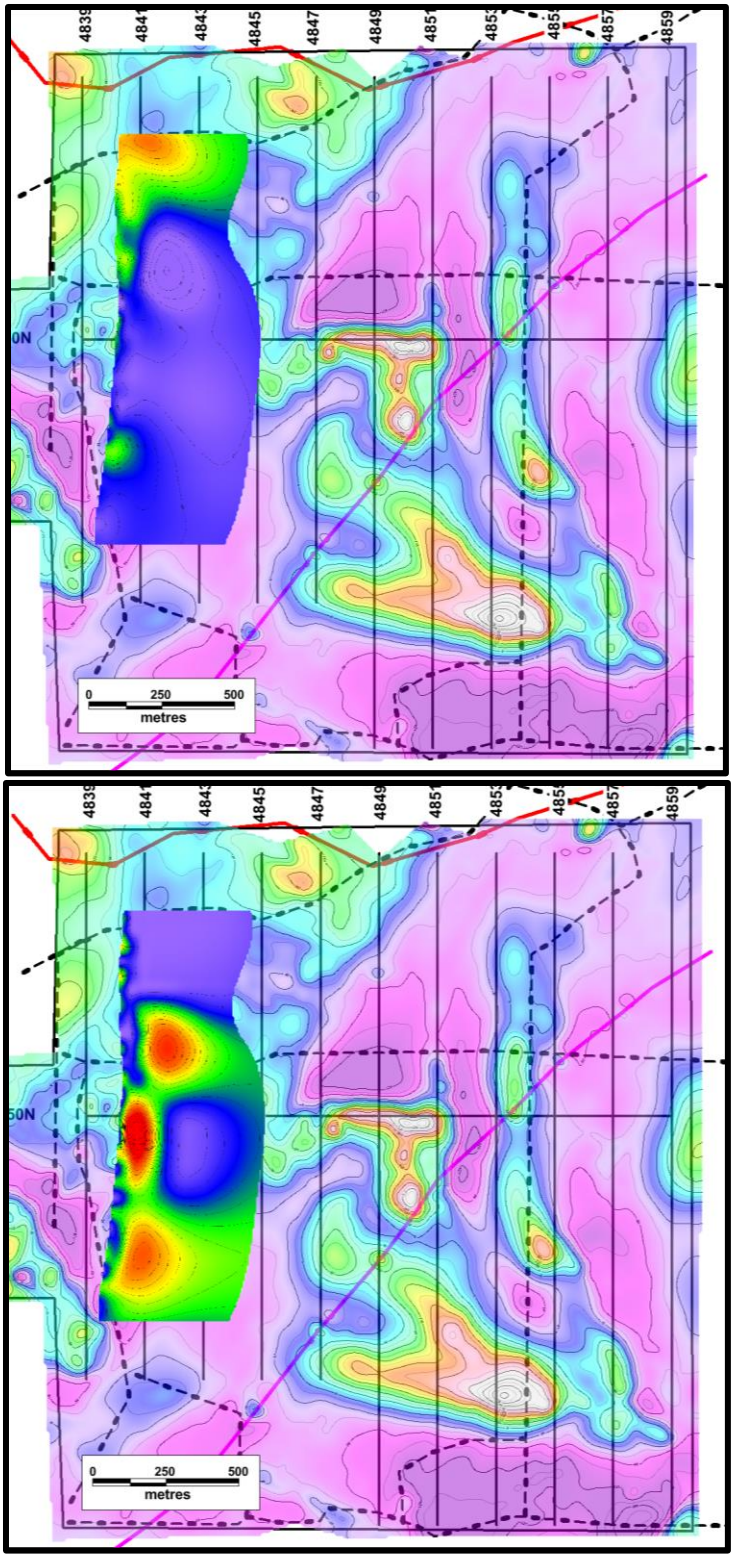

FIGURE 1: Line 483950E Inverted Section over Residual Magnetics (Resistivity – Upper / Chargeability – Lower)

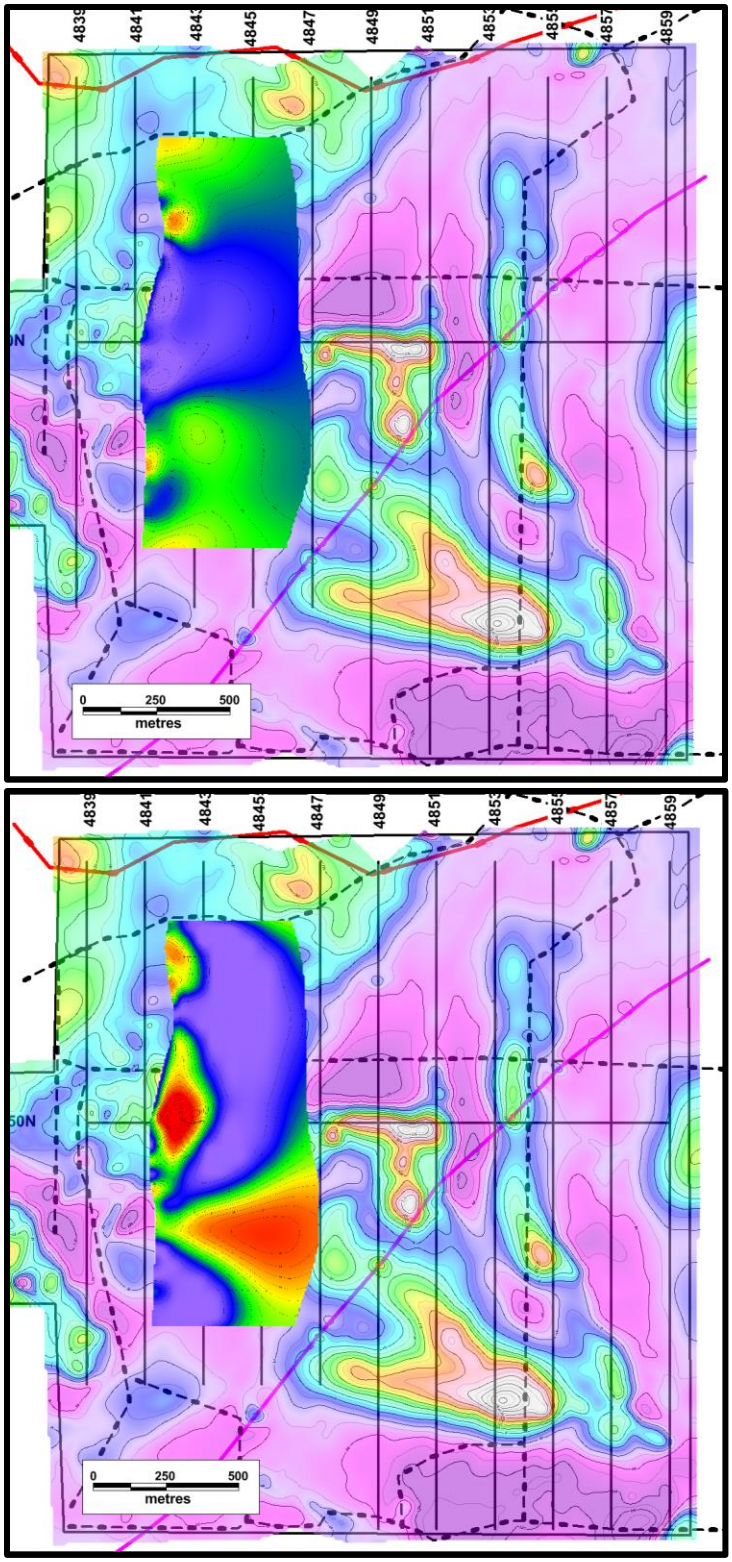

FIGURE 2: Line 484150E Inverted Section over Residual Magnetics (Resistivity – Upper / Chargeability – Lower)

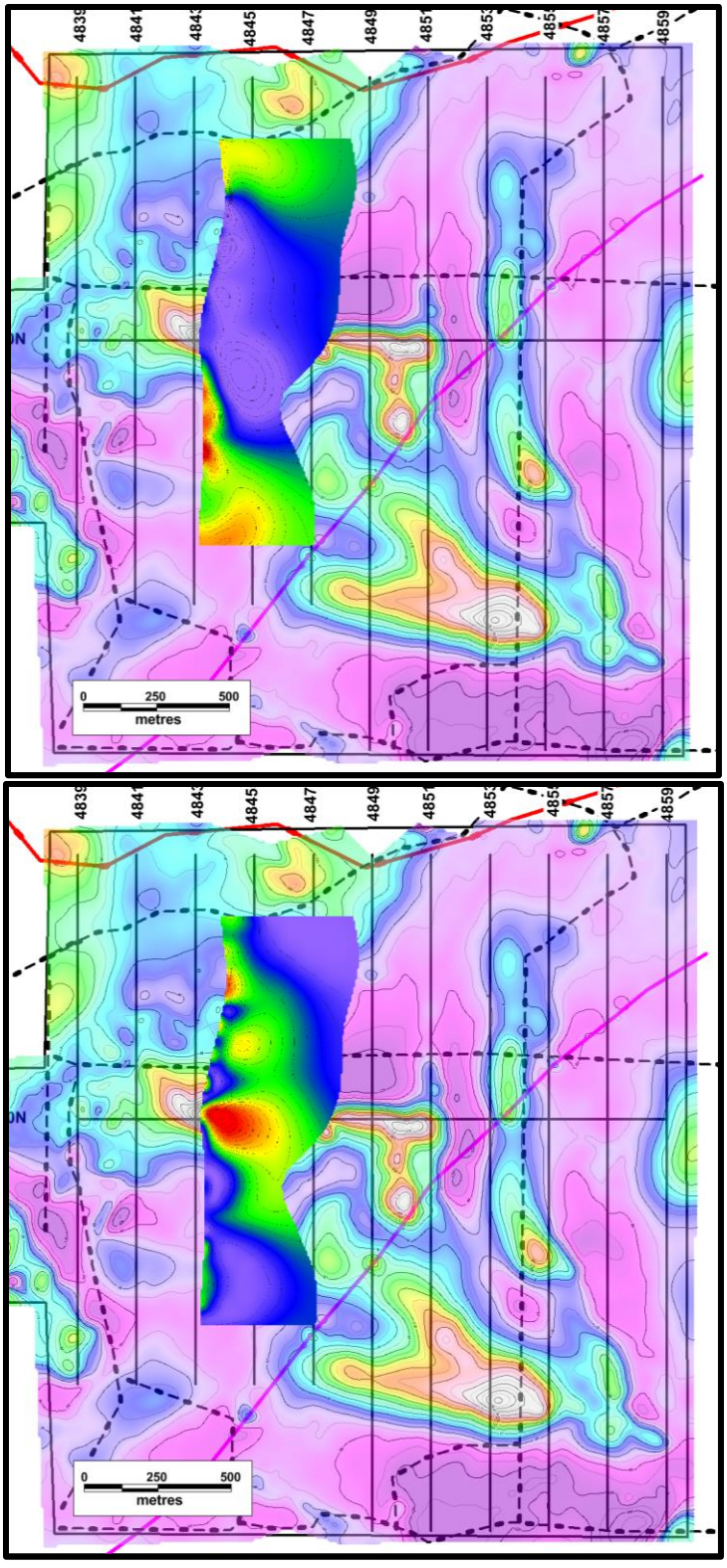

FIGURE 3: Line 484350E Inverted Section over Residual Magnetics (Resistivity – Upper / Chargeability – Lower)

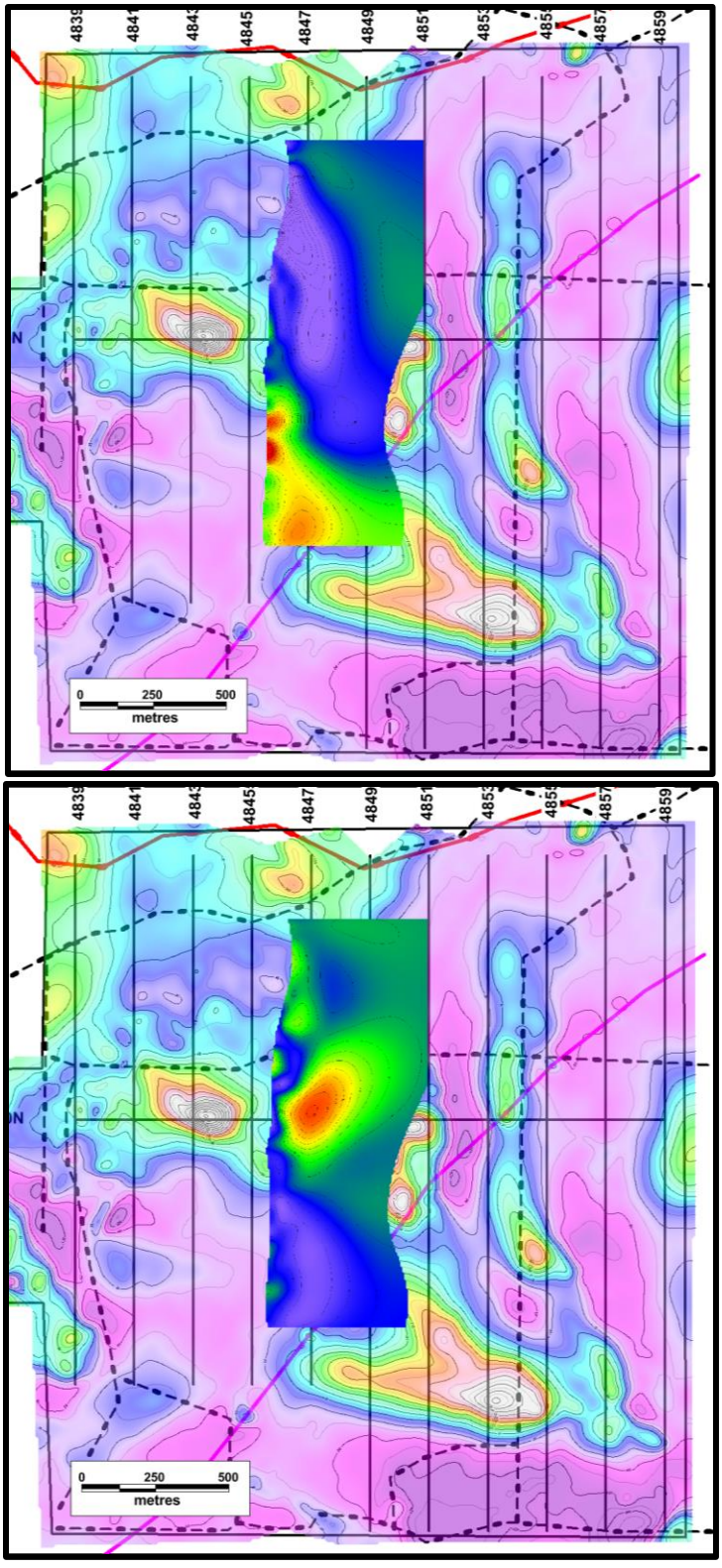

FIGURE 4: Line 484550E Inverted Section over Residual Magnetics (Resistivity – Upper / Chargeability – Lower)

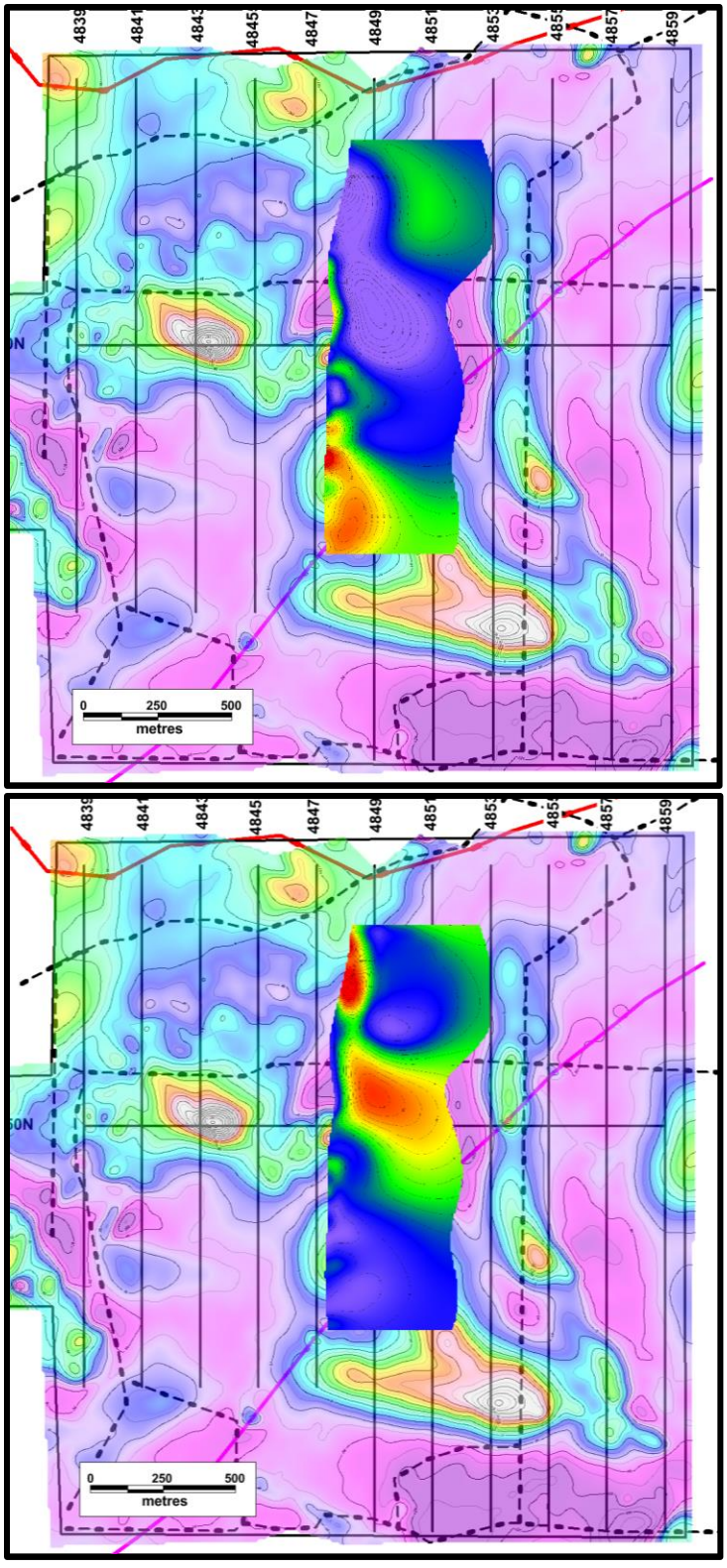

FIGURE 5: Line 484750E Inverted Section over Residual Magnetics (Resistivity – Upper / Chargeability – Lower)

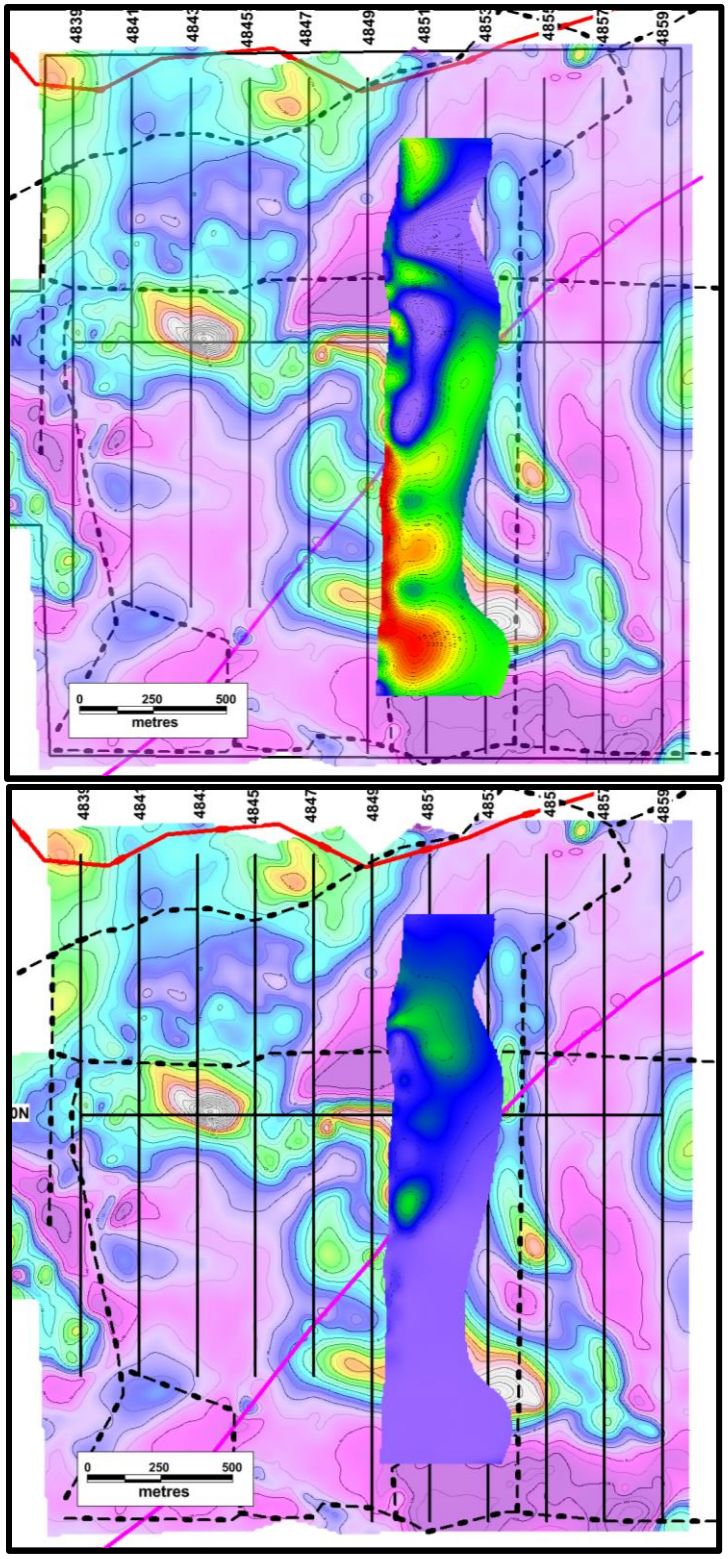

FIGURE 6: Line 484950E Inverted Section over Residual Magnetics (Resistivity – Upper / Chargeability – Lower)

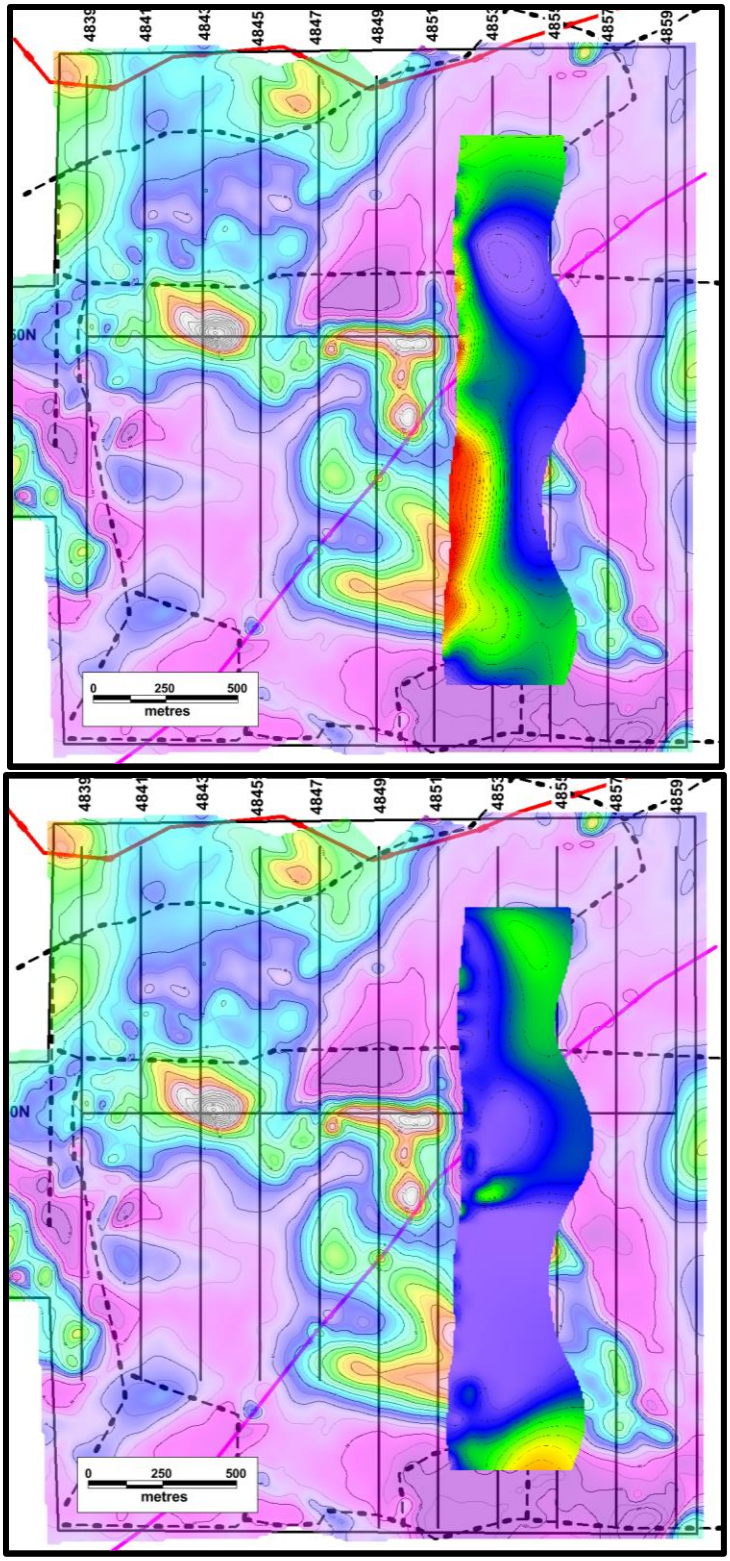

FIGURE 7: Line 485150E Inverted Section over Residual Magnetics (Resistivity – Upper / Chargeability – Lower)

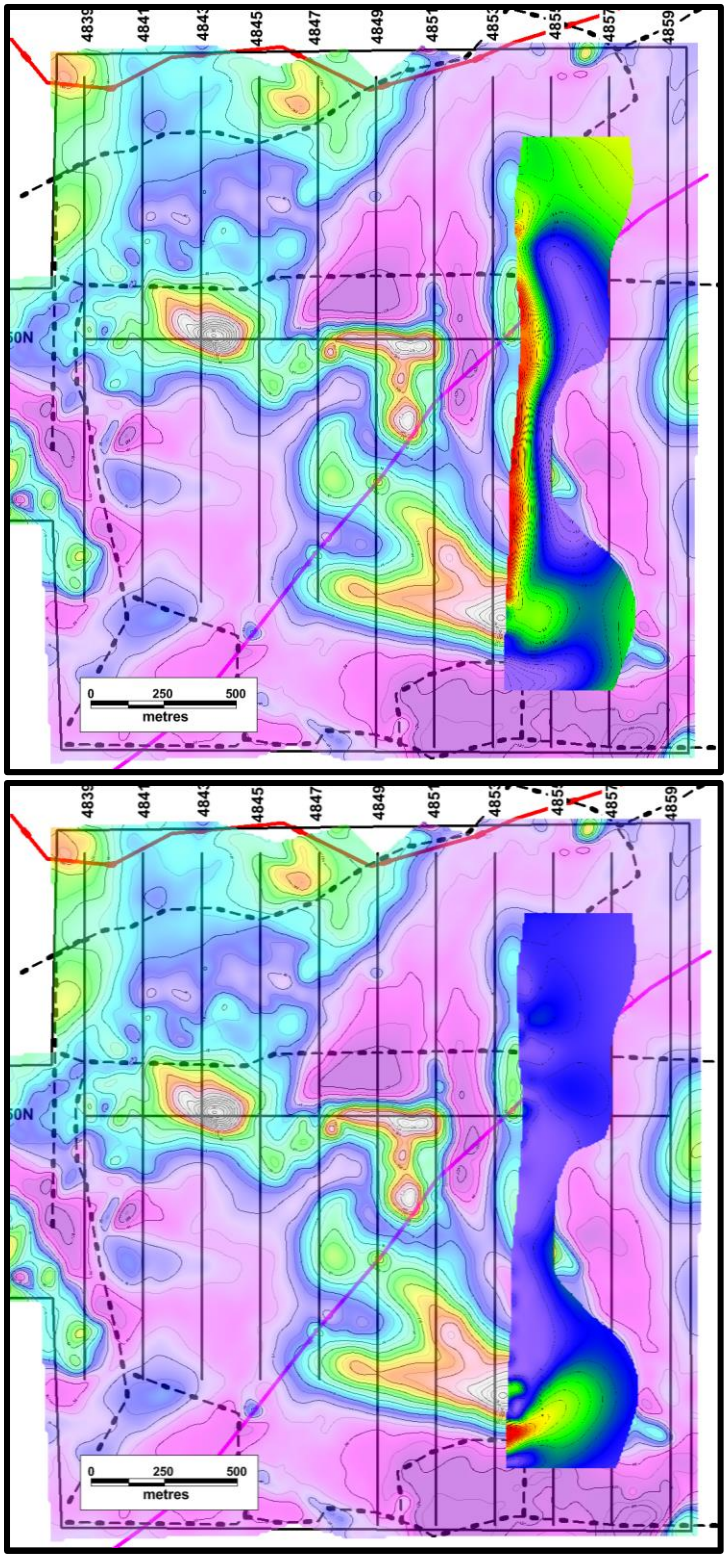

FIGURE 8: Line 485350E Inverted Section over Residual Magnetics (Resistivity – Upper / Chargeability – Lower)

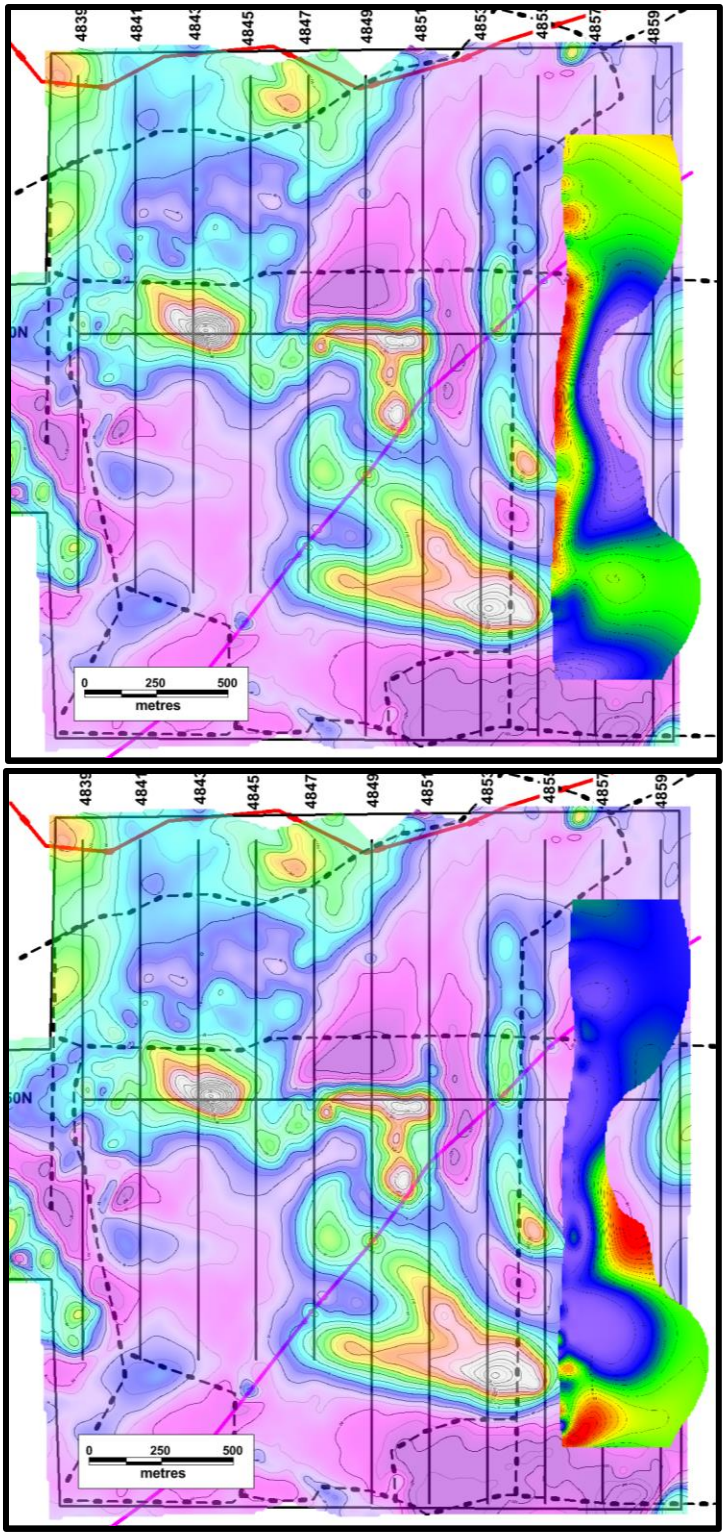

FIGURE 9: Line 485550E Inverted Section over Residual Magnetics (Resistivity – Upper / Chargeability – Lower)

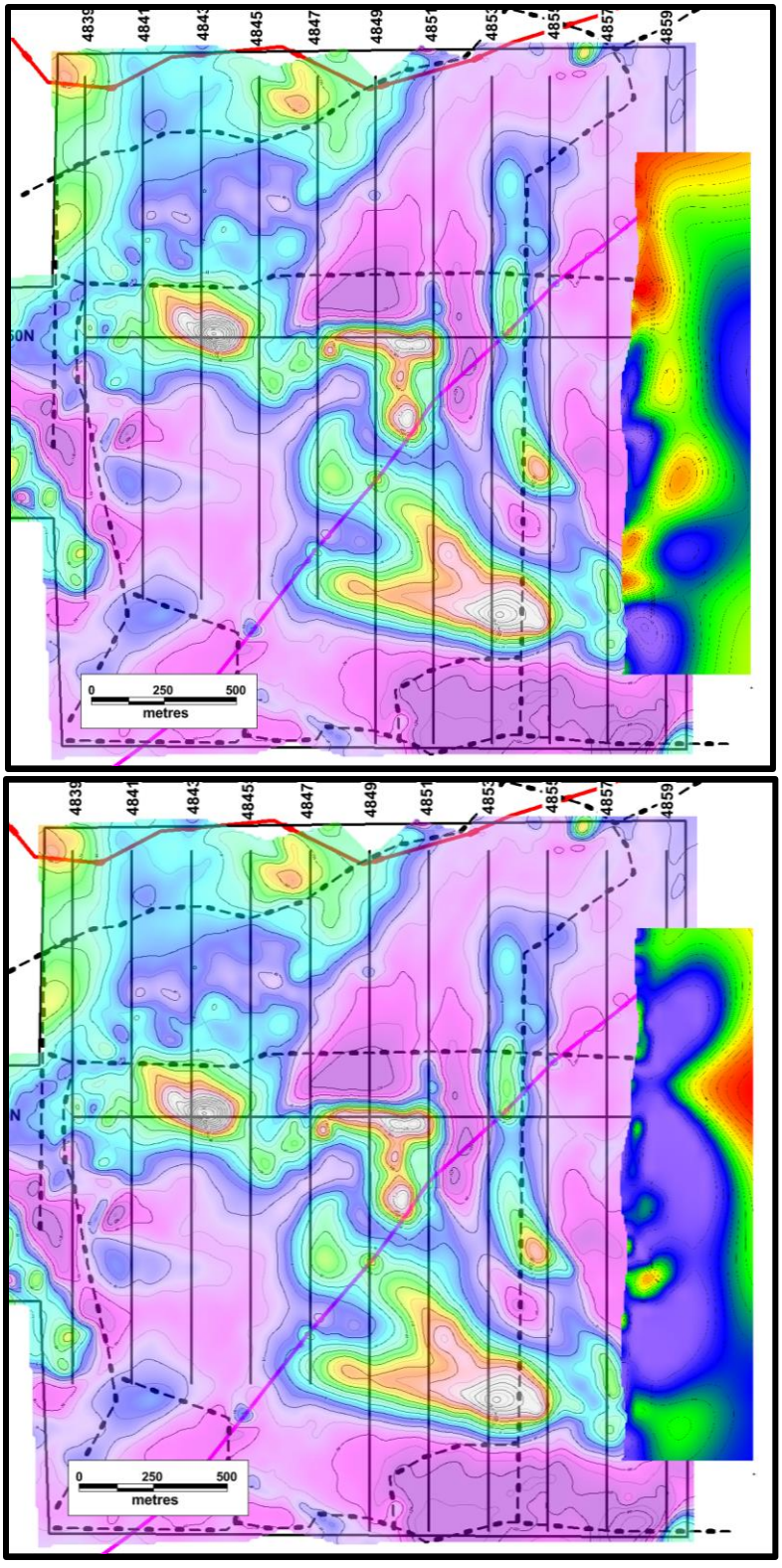

FIGURE 10: Line 485750E Inverted Section over Residual Magnetics (Resistivity – Upper / Chargeability – Lower)

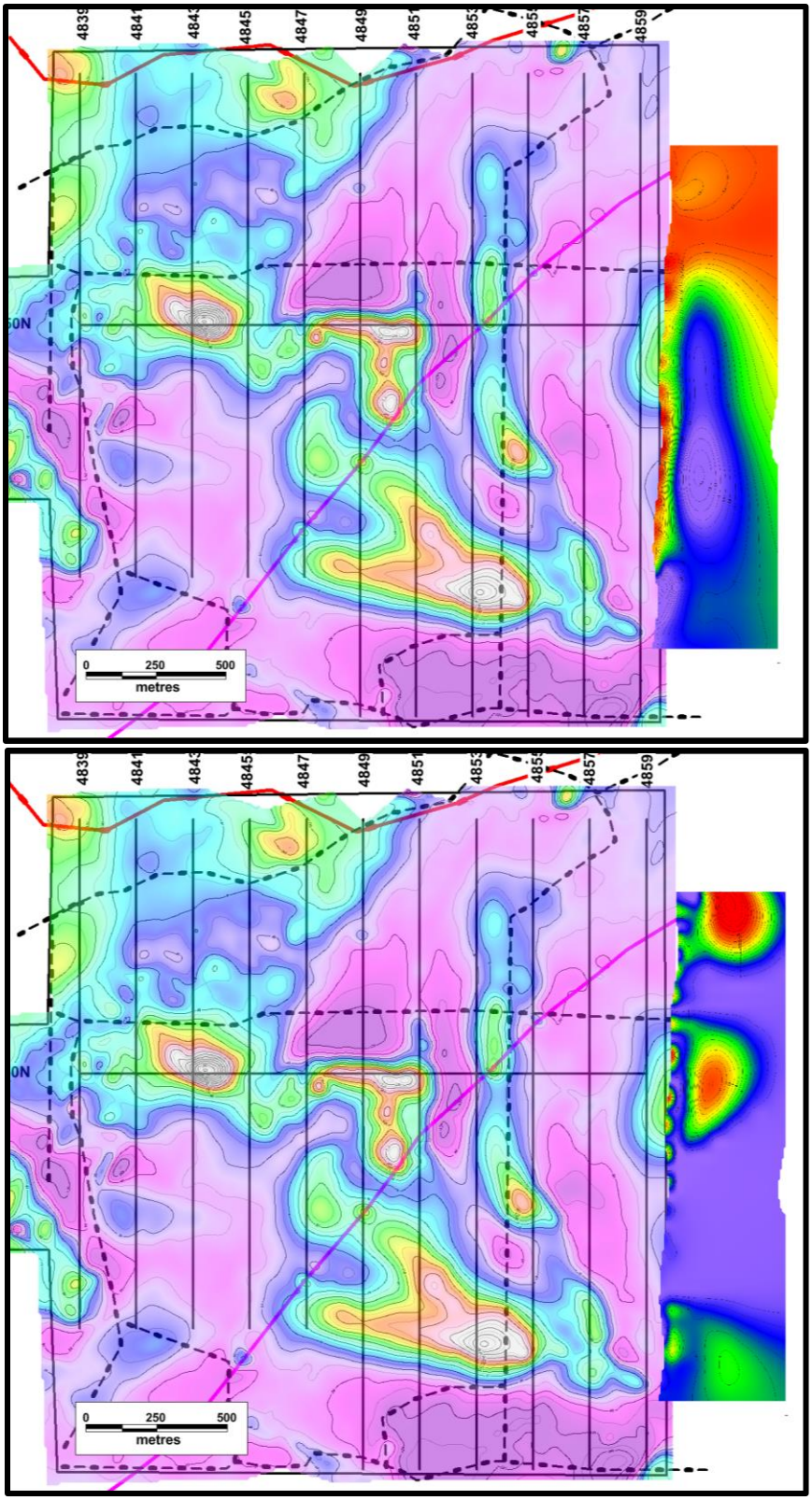

FIGURE 11: Line 485950E Inverted Section over Residual Magnetics (Resistivity – Upper / Chargeability – Lower)